

PHYSICS AND APPLICATIONS OF PHOTONIC CRYSTALS

A DISSERTATION

SUBMITTED TO THE DEPARTMENT OF PHYSICS
AND THE INSTITUTE OF ENGINEERING AND SCIENCE
OF BILKENT UNIVERSITY
IN PARTIAL FULFILLMENT OF THE REQUIREMENTS
FOR THE DEGREE OF
DOCTOR OF PHILOSOPHY

By

Barak Temelkuran

April, 2000

QC
793.5
-P427
T46
2000

PHYSICS AND APPLICATIONS OF PHOTONIC CRYSTALS

A DISSERTATION
SUBMITTED TO THE DEPARTMENT OF PHYSICS
AND THE INSTITUTE OF ENGINEERING AND SCIENCE
OF BİLKENT UNIVERSITY
IN PARTIAL FULFILLMENT OF THE REQUIREMENTS
FOR THE DEGREE OF
DOCTOR OF PHILOSOPHY

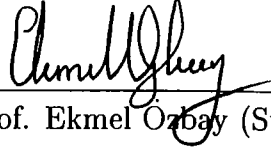
By
Burak Temelkuran

April, 2000

QC
793.5
.P427
T46
2000

B 052998

I certify that I have read this thesis and that in my opinion it is fully adequate, in scope and in quality, as a dissertation for the degree of Doctor of Philosophy.



Assoc. Prof. Ekmel Özbay (Supervisor)

I certify that I have read this thesis and that in my opinion it is fully adequate, in scope and in quality, as a dissertation for the degree of Doctor of Philosophy.



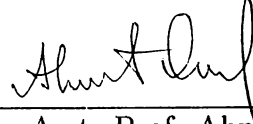
Prof. Alexander Shumovsky.

I certify that I have read this thesis and that in my opinion it is fully adequate, in scope and in quality, as a dissertation for the degree of Doctor of Philosophy.



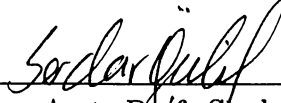
Prof. Çiğdem Erçelebi

I certify that I have read this thesis and that in my opinion it is fully adequate, in scope and in quality, as a dissertation for the degree of Doctor of Philosophy.



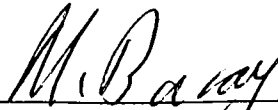
Asst. Prof. Ahmet Oral

I certify that I have read this thesis and that in my opinion it is fully adequate, in scope and in quality, as a dissertation for the degree of Doctor of Philosophy.



Asst. Prof. Serdar Özçelik

Approved for the Institute of Engineering and Science:



Prof. Mehmet Baray,
Director of Institute of Engineering and Science

ABSTRACT

PHYSICS AND APPLICATIONS OF PHOTONIC CRYSTALS

Burak Temelkuran

Ph. D. in Physics

Supervisor: Assoc. Prof. Ekmel Özbay

April 2000

We first fabricated a dielectric based layer-by-layer photonic crystal, with a three-dimensional photonic band gap at microwave frequencies. We investigated the transmission, reflection and defect characteristics of the crystal. A Fabry-Perot cavity analogy was used to understand the localization of the electromagnetic (EM) fields around defects. We then showed the enhancement of the EM field within the defect volumes, and suggested a possible application: resonant cavity enhanced detectors built around photonic crystals. We demonstrated that a detector inserted inside the defect volume benefits from the frequency selectivity and the highly enhanced field of the cavity. Next, we investigated the radiation of the EM fields from a source inserted in the defect volume, and observed that the radiated field has a very high directivity and efficiency. The experimental results agreed well with the theoretical expectations.

We demonstrated waveguiding structures built around photonic crystals. We showed that EM waves could be guided through a planar air gap between two photonic crystals, in which the wave is coupled inside the defect volume, and having no where else to go, propagates through this opening. The dispersion diagrams for these planar waveguide structures also agreed well with the theoretical expectations of our waveguide model. We also showed that, the wave could be guided along a single missing rod, and demonstrated the bending of the EM waves for these waveguide structures with “L” shaped openings.

We tested metallic photonic crystals built in different dimensions and different filling ratios. We observed many superiorities of these structures when compared to dielectric-based photonic crystals. A full characterisation of various metallic photonic crystals was performed. We also showed that metallic photonic crystals are suitable for some of the applications we have demonstrated for dielectric structures. We also fabricated a new layer-by-layer photonic crystal using highly doped silicon wafers processed by semiconductor micromachining techniques, with a band gap at millimeter wave frequencies. We showed that the transmission and defect characteristics of these structures are analogous to metallic photonic crystals, as we have predicted. The experimental results agree well with the predictions of the transfer matrix method (TMM) simulations. The method can be extended to fabricate these crystals at THz frequencies.

Keywords: Photonic Crystal, Photonic Band Gap (PBG), Defect, Fabry-Perot Cavity, Resonant Cavity Enhancement, EM Field Radiation, Directivity, Waveguide, Transfer Matrix Method (TMM), Doping, Semiconductor Micromachining.

ÖZET

FOTONİK KRİSTALLERİN FİZİĞİ VE UYGULAMALARI

Burak Temelkuran

Fizik Doktora

Tez Yöneticisi: Doç. Dr. Ekmel Özbay

Nisan 2000

Katmanlardan oluşan ve mikrodalga frekanslarında üç boyutlu fotonik bant aralığı gösteren bir fotonik kristal ürettik. Bu kristalin geçirgenlik, yansıtma ve düzensizlik özelliklerini inceledik. Fabry-Perot modeli benzetmesi kullanarak bu düzensizliklerde elektromanyetik dalgaların lokalize oluşunu açıkladık. Daha sonra yaratılan bu düzensizliklerin oluşturduğu boşluklarda elektromanyetik (EM) dalganın yükseltgendiğini göstererek olası bir uygulama önerdik: Fotonik kristallerde yaratılan rezonans kavite tarafından yükseltgenmiş detektörler. Düzensizlik içine yerleştirilen detektörün, bu kavitenin frekans seçiciliğinden ve kavite içindeki yükseltgenmiş alandan faydalandığını gösterdik. Bu tür düzensizliklerin içine yerleştirilen bir kaynaktan yayılan EM dalganın belirli bir yönde ve yükseltgenmiş alduğunu gözlemledik. Kuramsal ve deneysel sonuçların uyduğunu gördük.

Fotonik kristalleri kullanarak dalga kılavuzu yapmak için bazı önerilerde bulunduk. İki fotonik kristal arasında düzlemsel boşluk sayesinde, böyle bir düzensizliğe giren bir dalganın, gidecek başka bir yeri olmadığı için bu açıklık boyunca ilerlediğini gösterdik. Deneysel olarak bulduğumuz dalga vektörünün frekansa bağlı değişimi dalga kılavuzu modelimizin kuramsal sonuçlarıyla uydu. Bundan başka, dalganın fotonik kristalden çıkarılan bir çubuk boyunca da kayıp olmadan ilerlediğini gözlemledik ve bu dalga

kılavuzu yapılarıyla dalga'nın "L" şeklinde bir boşluktan kayıp olmaksızın dönebildiğini gösterdik.

Boyutları ve doluluk oranları deęişik bazı metalik fotonik kristal yapıları inceledik. Bu yapıların birçok yönden dielektirik fotonik kristallerden üstün olduğunu gözlemledik. Bu yapıların her türlü özelliklerini içeren genişbir inceleme yaptık. Ayrıca metalik fotonik kristallerin, dielektirik kristallerde de incelediğimiz bazı uygulama alanları için uygun olduğunu gösterdik. Yüksek katkılı silikon örnekleri kullanarak, yarıiletken mikro-şekillendirme yöntemleri ile, bant aralığı milimetre dalga boylarında olan yeni bir fotonik kristal ürettik. Bu yapının beklediğimiz gibi metalik özelliklere sahip olduğunu gösterdik. Deneysel sonuçlar, transfer matris metodu simülasyon sonuçlarıyla uyuyordu. Bu metod ile THz. frekanslarda bant aralığı olan fotonik kristaller kolayca üretilebilir.

Anahtar

sözcükler: Fotonik Kristal, Fotonik Bant aralığı, Düzensizlik, Fabry-Perot Kavitesi, Rezonans Kavite Yükseltgenmesi, EM dalga Yayılımı, Yön Seçimi, Dalga Kılavuzu, Transfer Matris Metodu, Katkılandırma, Yarıiletken Mikro-şekillendirme.

ACKNOWLEDGMENTS

I would like to express my sincere gratitude to Dr. Ekmel Özbay, whose personal and academic virtue greatly shaped my approach to scientific study. Beyond that, with his motivating and friendly attitude, I feel myself lucky to be **his** student during my graduate study.

Until the joining of Mehmet Bayındır to our group, I was the only and lonely PhD. student of Dr. Özbay. Thank you Mehmet, for coming. I would like to say that I really enjoyed his company, and the good time we spent in our laboratory, not to mention his help in the formation of this thesis work.

I would also thank to my friends and collaborators Ayhan Bozkurt and Sanli Ergun from EE department of Bilkent, who also did not leave me alone in the laboratory.

I would like to thank to the members of my dissertation jury for reading the manuscript and commenting on the thesis.

I am indebted to Prof. K. M. Ho, Prof. R. Biswas, Dr. M. M. Sigalas, Prof. C. M. Soukoulis, Prof. G. Tuttle, Dr. J. Kavanaugh from Iowa State University (ISU) for their hearty hospitality during my visits and their invaluable collaboration from such a long distance.

Being in the Physics Department of Bilkent University for 11 years, it is my pleasure to thank to all the people who was, is and will be a member of this department. My special thanks to Prof. Salim Çıracı and Prof. Cemal Yalabık, who came to our

highschool 11 years ago, and started everything persuading me to be a member of this department, and who gave the courage to continue at all times in my Bilkent life. The list continues with other professors who shared their invaluable knowledge with us; the secretaries who made our life easier; my ex-office mates (Talal Azfar and Erhan Ata), and my current office-mate Selim Tanrıseven, with whom I shared not only the room; all the undergraduate and graduate friends who helped me to prolongate good times and shorten bad times. I always felt better thinking that Murat Güre and Güngör “Abi” were there with their invaluable helps and friendships.

There is also a long list of my close friends, whether old or new, far away or nearby; to feel their existence is my life source. Thank you all!

I am also indebted to my mom, my dad and my brothers for their continuous support and encouragement. I would also thank to my new mom, dad and brothers, who doubled the support and encouragement I have.

And... thank you Canan, because you are Canan, and you are “here”.

When Albert Einstein discovered, in the first decade of the twentieth century, that enormous reservoirs of energy are latent in all matter, he at first rejected the suggestion that it might ever be possible to release that energy in a nuclear explosion. His essay entitled

$$“E=mc^2”$$

was written in 1946, by which time he and the world had become sadder and wiser.

Hoping that this work contributes to the peace of the world and happiness of the people, I dedicate this thesis



*to the pouring rain, shining sun,
to the blue colour of the sea ,
to the singing of a mermaid,
to the first smile of a baby,
to the smell and beauty of a rose.*

Contents

1	Introduction	1
1.1	Motivation	3
1.2	Summary of this work	7
2	Formation of Photonic Band Gap and Defects	8
2.1	Photonic band gap	8
2.2	Fabry-Perot analogy	11
2.3	Quality Factor	16
3	Resonant Cavity Enhanced Detectors	20
3.1	Detector inside planar cavity of photonic crystal	20
3.2	Fabry-Perot model	22
3.3	Tuning bandwidth	24
3.4	Box-like cavity	25
4	Highly Directional Resonant Antennas	27
4.1	Radiation patterns	28

4.2	Characterization	31
5	Waveguide Structures	34
5.1	Through waveguide	35
5.2	L-shaped waveguide	37
5.3	Two-dimensional waveguide	39
5.4	Dispersion diagrams	40
5.5	Guided waves through removed rods	42
6	Metallic Photonic Crystals	45
6.1	Crystal structure	45
6.2	Transmission properties of metallic photonic crystals	46
6.3	Defect structures in metallic photonic crystals	50
6.4	Resonant cavity enhancement	56
6.5	Directive radiation patterns from metallic photonic crystals	57
6.6	Towards lower filling ratios	58
7	Quasi-Metallic Silicon Micromachined P. C.	61
7.1	Fabrication Process	62
7.2	Characterization	65
8	Conclusion	70

List of Figures

1.1	Inhibition of the spontaneous emission	3
1.2	First 3-D photonic crystal	5
1.3	Layer-by-layer photonic crystal	6
1.4	Layer-by-layer structure is recently fabricated at optical frequencies. . . .	6
2.1	Experimental setup	9
2.2	Reflection and transmission characteristics	10
2.3	The reflection phase from the photonic crystal	11
2.4	Transmission from a single rod removed defect structure	11
2.5	Transmission of planar defect structures	12
2.6	The Fabry Perot model	13
2.7	Phase comparison	15
2.8	Double defect formation	16
2.9	High q factor defect mode	17
2.10	Comparison of inverse Q factor and Transmission	18

3.1	Experimental enhancement factor obtained for planar defect structure using network analyzer.	21
3.2	Experimental enhancement factor obtained for planar defect structure using microwave detector.	22
3.3	Schematics of the Fabry-Perot cavity model	23
3.4	Comparison of experiment and theory	24
3.5	Tuning bandwidth of RCE detector	25
3.6	Enhancement characteristics of the box like cavity.	26
4.1	Experimental setup for measuring the radiation patterns	29
4.2	Measured and calculated radiation patterns	30
4.3	Detected and reflected power characteristics of antenna	33
5.1	Light turning through a sharp bend within the photonic crystal	35
5.2	Experimental setup for waveguide measurements	36
5.3	Transmission amplitude measured from parallel-plate waveguides	36
5.4	Transmission through a narrow-width L-shaped waveguide	38
5.5	Transmission through a wide-width L-shaped waveguide	38
5.6	2D waveguide transmission characteristics	39
5.7	Vector diagram of the EM wave propagating inside the waveguide	41
5.8	Theoretical and experimental dispersion diagrams	42
5.9	The schematics and corresponding transmission characteristics of waveguides created by missing rods	44

6.1	Schematics of fct and st based metallic photonic crystals	46
6.2	Transmission characteristics of metallic photonic crystals	47
6.3	Rejection rates	47
6.4	Comparison of the measured transmission amplitude with the simulation result.	48
6.5	Transmission measurement with monopole antenna	49
6.6	Transmission characteristics of a 14 layer st based crystal with a single rod removed defect.	50
6.7	Transmission characteristics of an 18 layer st based crystal with a single rod removed defect	51
6.8	The defect characteristics of a 14 layer fct based crystal with a single rod removed defect structure.	51
6.9	The tuning of the defect frequency in planar defect structures	52
6.10	Q factor as a function of inverse transmission	53
6.11	High Q factor defect mode	53
6.12	Comparison of measured and simulated defect characteristics of st structure	54
6.13	Transmission at various angles from crystal with planar defect	55
6.14	Enhancement characteristics of a planar defect structure	56
6.15	Radiation patterns from a monopole antenna inside metallic photonic crystals	57
6.16	Transmission properties of low filling ratio (a) fct and (b) st based crystals.	59
6.17	Defect characteristics of low filling ratio metallic photonic crystals	60

7.1	Schematics of the process steps	63
7.2	W-band experimental setup.	65
7.3	The transmission characteristics of st crystal	66
7.4	The transmission characteristics of fct crystal	66
7.5	Reflection and transmission from a ten layer st type photonic crystal. . .	67
7.6	Measured and simulated transmission characteristics of st type crystal . .	67
7.7	Transmission characteristics of 9 layer fct type of crystal with a single rod removed defect.	68
7.8	Transmission characteristics of layer fct type of crystal with a planar defect	69
7.9	Comparison of simulated defect characteristics for different doping concentrations with experimental results.	69

List of Tables

2.1	Experimental measured defect frequencies and corresponding phase values for different separation widths.	14
-----	---	----

Chapter 1

Introduction

Optics is a very old subject, as old as the times the cave men started a settled life. The processed oxidien stones unearthed in Çatalhöyük in central Turkey, are believed to be used as mirrors at those times (~ 6000 BC). A mirror formed with a more scientific approach is the bronze one which was used together with water (~ 3000 BC).¹ The content of optics is the generation, propagation and detection of light. The three major developments in the last forty years; invention of laser, fabrication of low loss optical fibers, and introduction of semiconductor optical devices were the main reasons in the improvement of interest on optics, both in basic research and in modern technology.

In recent years, by the increase in the connection between optics and electronics, the term photonics has come into use, in analogy to the term electronics. Electronic systems are designed to control the flow of electric-charge, while controlling the propagation of light is the subject of photonics.

The analogy goes further than the description itself, when we consider the equations describing behaviours of electrons and photons.^{2,3} The Schrödinger equation describes behaviour of electrons in a space variant potential $V(\mathbf{r})$:

$$\left\{ -\frac{\hbar^2}{2m^*} \nabla^2 + V(\mathbf{r}) \right\} \Psi(\mathbf{r}) = E\Psi(\mathbf{r}) \quad (1.1)$$

where \hbar is the Planck constant divided by 2π , m^* is the effective electron mass, $\Psi(\mathbf{r})$ is the scalar wave function, and E is the energy eigenvalue.

The periodicity of atoms in a crystal structure is something that was formed naturally. This periodicity, entering the Schrödinger equation as a periodic potential had played the major role in this century's most important development in technology, introduction of semiconductor devices. The periodicity resulted in an energy band gap, in which any propagating electron state is strictly forbidden. Using these properties, people were able to control and manipulate the flow of electric charge. The formation of the band gap can be thought as Bragg-type of reflections from periodic atomic structures, when the wave nature of the electron is considered. Similarly, propagation of an electromagnetic (EM) wave can be blocked using a periodic structure. The idea becomes more clear when we write the Maxwell equation for a propagating EM waves in a dielectric media with a space-variant dielectric function⁴:

$$\left\{ -\nabla^2 - \frac{\omega^2}{c^2} \epsilon_{fluct}(\mathbf{r}) \right\} \mathbf{E}(\mathbf{r}) + \nabla (\nabla \cdot \mathbf{E}(\mathbf{r})) = \epsilon_0 \frac{\omega^2}{c^2} \mathbf{E}(\mathbf{r}) \quad (1.2)$$

where ω is the angular frequency of the field, and c is the speed of light in free space. Except the term $\nabla(\nabla \cdot \mathbf{E})$, the analogy between the Schrödinger equation and the Maxwell equation is obvious. The total dielectric constant in the second equation is separated as $\epsilon(\mathbf{r}) = \epsilon_0 + \epsilon_{fluct}(\mathbf{r})$, into its average value ϵ_0 and a spatially fluctuating part $\epsilon_{fluct}(\mathbf{r})$. The latter plays a role analogous to the $V(\mathbf{r})$ in the Schrödinger equation, and the quantity $\epsilon_0 \omega^2 / c^2$ plays the role of the energy eigenvalue E of the Schrödinger equation.

It can be understood from the above equation that an artificially created three-dimensional periodic dielectric structure results in a photonic band gap (PBG), in which the propagation of the EM wave is strictly forbidden regardless of the direction in a certain frequency range.⁵ The PBG, which is only a decade old, is the key to the idea that leads to control and manipulation of light. There had been a great deal of interest in this research during the last few years. The results of these researches came along with numerous applications of these crystals in a spectrum extending from microwave to optical frequencies.⁶⁻¹⁶

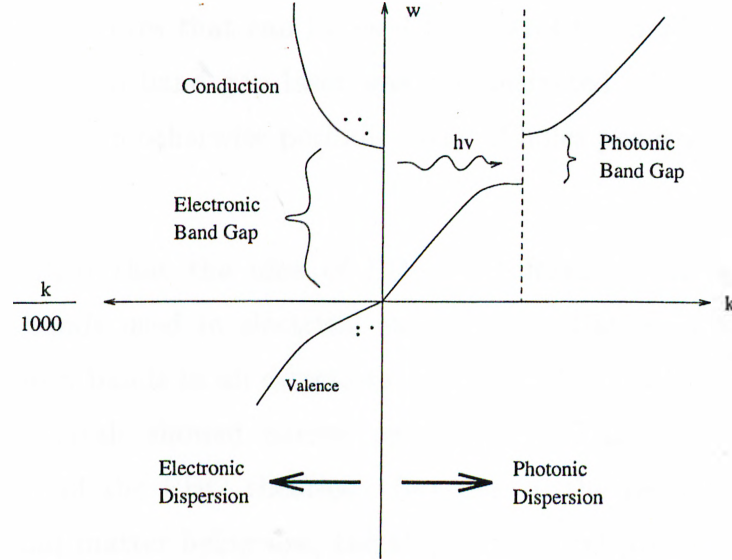


Figure 1.1: The dispersion relation for EM waves (right side), and the dispersion relation for electron waves of a typical direct-gap semiconductor (left side).¹⁷

1.1 Motivation

The control of spontaneous emission plays an important role in many applications based on quantum electronics and quantum optics. Many corresponding examples can be found. The threshold of a laser, the current gain in heterojunction bipolar transistors, and the maximum available output voltage in solar cells, all depend on the spontaneous recombination of electrons and holes. In 1987, Eli Yablonovitch suggested that the spontaneous emission can be inhibited using photonic crystals which do not allow propagation of the EM waves.⁵ Figure 1.1 shows how the spontaneous emission can be controlled by a photonic crystal.¹⁷ In a semiconductor, a photon is emitted by the recombination of an electron in the valence band with a hole in the conduction band. However, if a photonic crystal is designed to have a band gap covering the frequency of the emission, the photon will have no mode to couple, and recombination will simply be inhibited.

One other important issue of the photonic crystals is that, just like the donor or acceptor states in an electronic crystal, breaking the periodicity of the crystal results in

localization of the EM field within the defect volume.¹⁸ With these properties, photonic crystals are novel structures that can be used to control the behaviour of light.¹⁹ Very recently, two-dimensional band gap laser was demonstrated. The cavity consisted one filled hole (a defect) in an otherwise periodic array of holes penetrating a light emitting, semiconducting film.^{20,21}

It should be noted that the idea of PBG is different from the concept of one-dimensional stop bands used in electrical engineering. Rather, photonic crystals are expected to have stop bands in all directions. Early studies made on X-ray diffractions from natural fcc crystals showed narrow stop bands. This idea acted as the basis in the development of the PBG theories. But due to the refractive-index difference between vacuum and matter being low, the stop bands that are observed were narrow. Calculations showed that with refractive-index difference higher than 2, these stop bands may be opened to cover all directions in reciprocal space.²²

Due to technological difficulties, the fabrication of these crystals were initially restricted to microwave and millimeter-wave frequencies. The early PBG studies concentrated on testing various fcc type fabricated crystals.²³ By the introduction of vector wave calculations, scientists proved that the early structures did not have a full band gap due to band crossing along W direction of the Brillouin zone.^{24,25} The problem of band crossing was solved by a diamond structure suggested by the Iowa State group of Ho *et al.*²² This predicted structure was later fabricated by drilling a solid dielectric material from three different angles, each 35.26° away from the normal and spread 120° on the azimuth.²³ The crystal in the end was a full 3-D fcc structure with roughly cylindrical void atoms. This was the first experimental photonic crystal that possessed 3-D stop band. Along $\langle 111 \rangle$ direction, a gap extending from 13 GHz to 16 GHz was observed, with around 50 dB attenuation.

After this verification of the existence of photonic crystals, there was an increased effort in this research area. Scientists searched for new structures that could be more easily fabricated, and could be scaled down to optical frequencies. A new crystal that meets these requirements was invented by the Iowa State group.^{26,27} The designed

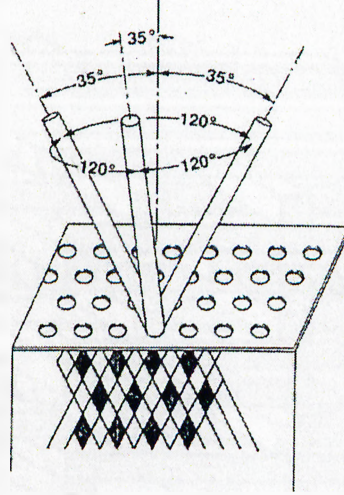


Figure 1.2: The drilling technique used in the construction of the first photonic crystal that possessed 3-D PBG.²³

structure, which was called layer-by-layer photonic crystal, has 3-D PBG, and could also easily be scaled to lower dimensions. Each layer of crystal was formed by dielectric rods arranged parallel to each other separated by a distance a . As seen in figure 1.3, each layer is stacked to the previous one by rotating the layer 90° with respect to the previous layer. Every third layer is parallel to the first one with a shift of $a/2$ in the direction perpendicular to the rods. The fourth layer is shifted the same way with respect to the second layer. So a unit cell of 4 layers of length c , where every fifth layer repeats the first one, is obtained. The angle between adjacent layers may vary from 90° to 60° . The structure has the symmetry of a face centered tetragonal (fct) type of structure. The crystal can be derived from a diamond structure if 110 chains of atoms were to be replaced by dielectric rods for the special case of $c/a = \sqrt{2}$.

This structure is important in the sense that, its dimensions could easily be lowered. Using the anisotropic etching property of Si by KOH, the layers of these crystals were prepared by micromachining techniques at lower scales. First a gap around 100 GHz was reached.²⁸ Then dimensions were further scaled down to achieve a photonic crystal with a full band gap around 500 GHz.²⁹ By using special silicon thinning methods and double etching the wafers from both faces, this technique could be extended to have photonic

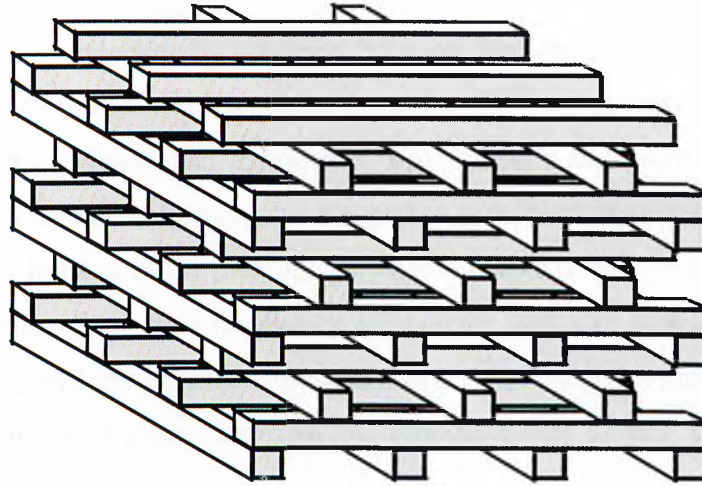


Figure 1.3: The design of an fct type of layer-by-layer crystal with a 3-D PBG. The structure is built by an orderly stacking of dielectric rods

band gaps around 20 THz.³⁰

Using advanced semiconductor processing techniques, this 3-D layer-by-layer structure is recently fabricated at optical frequencies (see Fig. 1.4).³¹⁻³⁵ With this breakthrough, the application of these crystals at optical frequencies is now feasible.

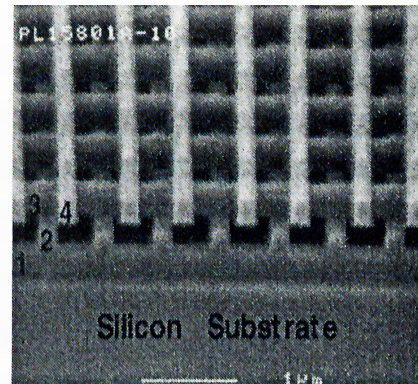
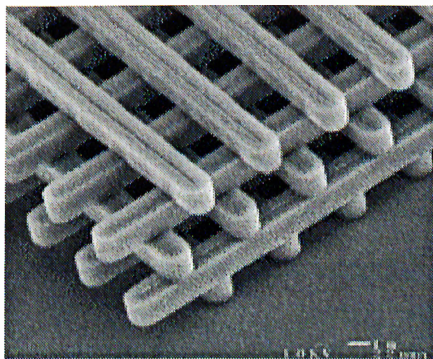


Figure 1.4: Layer-by-layer structure is recently fabricated at optical frequencies.

1.2 Summary of this work

We will first present a dielectric based layer-by-layer photonic crystal. The transmission, reflection and defect characteristics of the crystal will be investigated. A model will be proposed to understand the defect formation. We will then show the enhancement of the EM field within the defect volumes, and suggest a possible application: resonant cavity enhanced detectors built around photonic crystals, where a detector inserted inside the defect volume benefits from the frequency selectivity and the highly enhanced field of the cavity. Next, we will investigate the radiation of the EM fields from a source inserted in the defect volume, and show that the radiated field has a very high directivity and efficiency.

We will propose waveguides built around photonic crystals. We will show that EM waves could be a guided within a planar waveguide, in which the wave is coupled inside the defect volume, and having no where else to go, propagates through the opening carved through the crystal. The dispersion diagrams for these planar waveguide structures will also be presented, which agrees well with the theoretical expectations. We will also demonstrate the propagation of the EM waves through a single missing rod of the photonic crystal. We will show that the trapped waves may be guided even through a tight corner for these waveguide structures.

We will show that, the metallic structures built in different dimensions and different filling ratios have many superiorities when compared to dielectric-based photonic crystals. A full characterisation of various metallic photonic crystals will be presented, and some possible applications for metallic photonic crystals will be exhibited. A new method to fabricate quasi-metallic photonic crystals using semiconductor micromachining techniques will be demonstrated. The results and advantages of the new structure will be discussed.

Chapter 2

Formation of Photonic Band Gap and Defects

We constructed a photonic crystal having the geometry of layer-by-layer structure we have described in the previous section. The size of the crystal was chosen to be large for the purpose of easy fabrication, modification and measurement. In this chapter, we will introduce the basic characteristics of the new crystal. First, the band gap will be presented using the transmission and reflection results. Then, the properties of the defects built around this structure will be investigated, and a model to understand the defect formation will be proposed.³⁶

2.1 Photonic band gap

The layer-by-layer photonic crystal was constructed using alumina rods with a dielectric constant of 3.1 at 12 GHz, with the dimensions $0.32\text{cm} \times 0.32\text{cm} \times 15.25\text{cm}$. In this crystal, we chose a center to center separation of 1.12 cm, corresponding to a filling ratio of ~ 0.29 . Figure 2.1 shows the schematics of the measurement set up we used in our experiments.

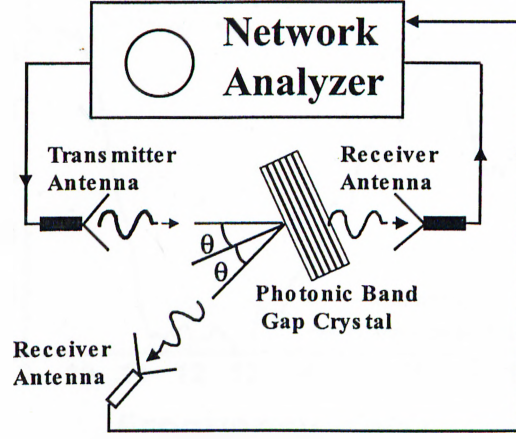


Figure 2.1: Experimental setup for the simultaneous measurement of reflection and transmission from a photonic crystal.

An HP8510C network analyzer and three microwave horn antennas were used to measure both the transmitted and reflected waves. For reflection measurements, we used a metal sheet to calibrate our measurements, where we assumed that the metal sheet is a 100% reflector at these frequencies. By changing the incidence angle θ , we could obtain the reflection and transmission properties of the photonic crystals at different propagation directions. By using the aforementioned experimental setup, we first investigated the transmission properties of our photonic crystal. The band gap edge values obtained from our transmission measurements along different crystal directions, were very close to the theoretical calculations which predicted a full band gap from 10.6 to 12.7 GHz.²⁶ We then focused our efforts on the reflection measurements.

Although, it was relatively easy to obtain the magnitude of the reflected waves on a reproducible basis, we faced a significant challenge to obtain reproducible phase measurements where we used a metal sheet for calibration purposes. The flatness of the top surface of the photonic crystal and the positioning of the photonic crystal with respect to the calibration metal plate were very critical for a reliable measurement. In our setup, our typical calibration error for the phase measurements was measured to be around $\pm 5^\circ$. Figure 2.2 shows the reflection and transmission characteristics of a 16

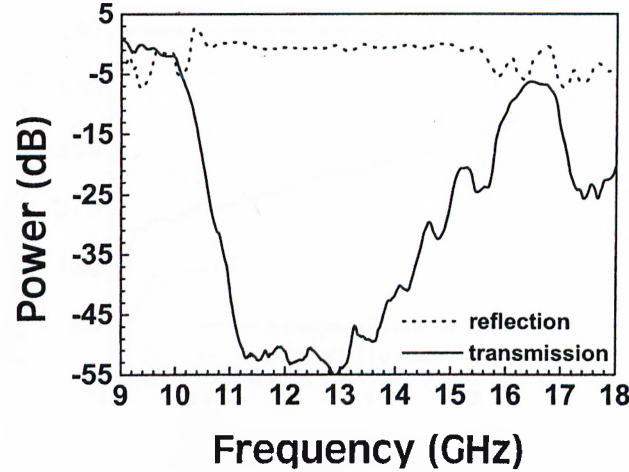


Figure 2.2: Reflection (dotted line) and transmission (solid line) along the stacking direction.

layer crystal along the stacking direction with an incidence angle 5° . The magnitude of the reflected and the transmitted waves were found to be independent of the polarization vector \mathbf{e} of the incident EM wave. However, we found a strong polarization dependence for the phase of the reflected waves. Figure 2.3 shows the phase of the reflected waves as a function of frequency for both polarizations where the polarization vector \mathbf{e} of the incident EM wave is either perpendicular or parallel to the rods of the top layer of the photonic crystal.

We have discussed the possibility of creating evanescent modes within the photonic band gap by breaking the periodicity of a photonic crystal. Figure 2.4 shows the transmission through a 16 layer crystal with a single missing rod from the 8th layer. A peak in the transmission is observed within the band gap corresponding to a localized mode at a resonant frequency of 12.16 GHz. The quality factor Q factor (quality factor) defined as the center frequency divided by the peaks full width at half maximum, is 1380, and the peak transmission maximum is 17.7 dB below the incident signal. The polarization vector \mathbf{e} of the EM field was parallel to the axis of the missing rod. The measurements done for the other polarization showed no resonances.

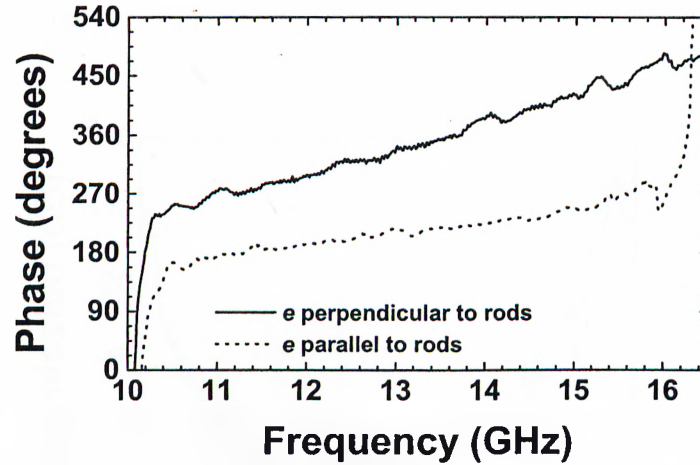


Figure 2.3: Experimental reflection phase properties of the photonic crystal for different polarizations.

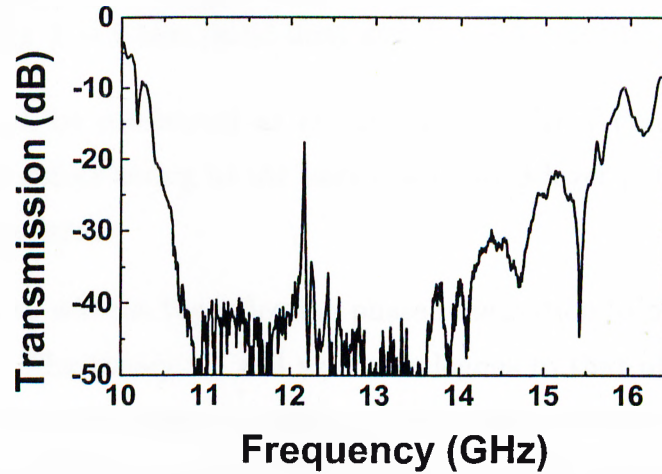


Figure 2.4: Transmission through a 4 unit cell photonic crystal with a single rod missing at the eight layer.

2.2 Fabry-Perot analogy

One other way to create defects in this structure is to introduce a planar air gap within the crystal. By separating a 16 layer photonic crystal from the middle with a separation width of L , we built planar defect structures. The transmission through this structures with $L = 6$ mm (solid line) and $L = 8.5$ mm (dotted line) are given in figure 2.5. As

seen from the figure, we can tune the frequency of the defect mode by simply changing the width of the cavity.

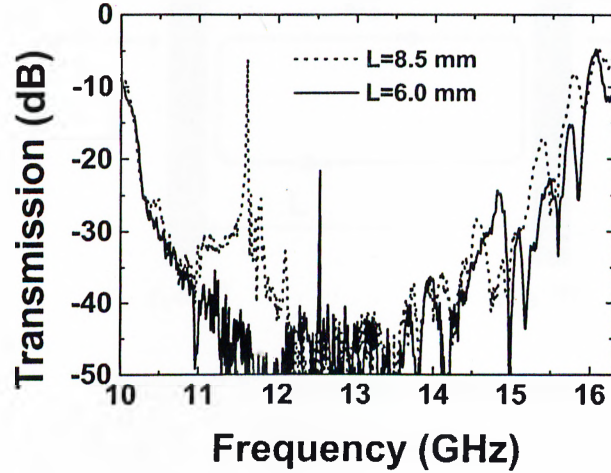


Figure 2.5: Transmission through 4 unit cell photonic crystal with a planar air gap at the middle of width $L = 6$ mm (solid line) and $L = 8.5$ mm (dotted line).

Our system can be considered as an analog of a Fabry-Perot resonator, with the introduced planar defect acting as the cavity, and the 8-layer photonic crystals on each side acting as the mirrors.

At this point, we will use the reflection phase information to predict the frequency of the defect modes. The theory we will use is analogous to that of the Fabry-Perot type of resonators.³⁷ In this analogy, to find the circulating field E_c inside the crystal, we add the transmitted field through the front mirror, and the reflected component after a round trip inside the cavity:³⁷

$$E_c = jt_1 E_i + r_1 r_2 e^{-j(2\beta L + \phi_1 + \phi_2)} E_c \quad (2.1)$$

where E_i is the initial wave, t_1 is the transmission coefficient of the front mirror, $r_1 e^{-j\phi_1}$ and $r_2 e^{-j\phi_2}$ are the reflection coefficients of mirrors, ϕ_1 and ϕ_2 are the reflection-phase factors in radians, β is the propagation constant for the travelling EM wave in air, and L the separation length of the cavity (Fig. 2.6). So, the ratio of the circulating field to the initial field can be calculated as:

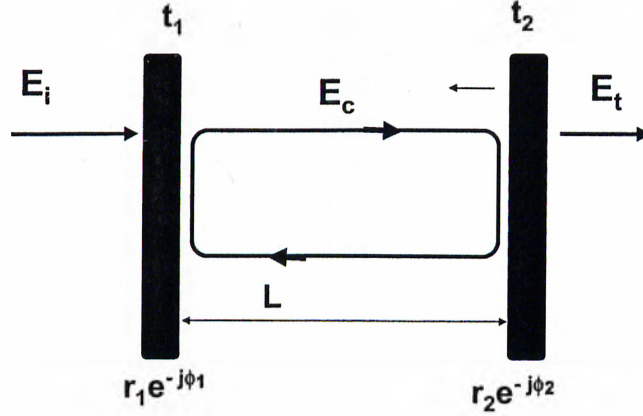


Figure 2.6: The Fabry Perot model

$$\frac{E_c}{E_i} = \frac{j t_1}{1 - r_1 r_2 e^{-j(2\beta L + \phi_1 + \phi_2)}} \quad (2.2)$$

The resonance condition is satisfied when the phase shift due to one round trip is a multiple of 2π , that is when $2\beta L + \phi_1 + \phi_2 = 2m\pi$ ($m = 0, \pm 1, \pm 2, \dots$). This resonance condition with the obtained reflection-phase information, can now be used to predict the frequency of the defect mode.

Changing the separation length L of the resonator, we obtained the transmission properties and the frequencies of the defect mode. The defect modes, first appearing at the upper band edge, shifts to the lower band edge of the stop band, as the separation length L is increased. If the separation is further increased to 10.0 mm., we start to observe secondary defects appearing at the upper band edge. In the mean time, the first defect shifts further down to lower frequencies to disappear at the lower band edge. To make a comparison of the theory with the experiment, we added the reflected phase measured from the two walls of the cavity $\phi_{t,ex} = \phi_1 + \phi_2$. Then, we compared it with the phase that should correspond to the defect frequency in the resonance condition which is given as,

Separation width L (mm)	Frequency GHz $m=1$	$\phi_t(f_L)$ (degrees) $m=1$	Frequency (GHz) $m=2$	$\phi_t(f_L)$ (degrees) $m=2$
3	13.97	260		
4	13.50	230		
5	13.13	202		
6	12.54	170		
7	12.15	156		
8	11.78	134		
9	11.45	113		
10	11.16	92	15.34	352
11	10.86	73	15.01	324
12	10.66	53	14.66	298
13	10.45	34	14.31	274
14			13.98	250

Table 2.1: Experimental measured defect frequencies and corresponding total phase contributions from the walls of the cavity for resonance condition are given for different separation widths, for the first ($m=1$) and second ($m=2$) defect modes.

$$\phi_t(f_L) = 2m\pi - 4\pi L \frac{f_L}{c} \quad (m = 0, \pm 1, \pm 2, \pm 3, \dots) \quad (2.3)$$

where f_L is the measured defect frequency corresponding to the separation width L . Table 2.1 lists the measured frequencies of the defect modes, the value of m and the calculated $\phi_t(f_L)$ as a function of separation length L . In figure 2.7, the predicted $\phi_t(f_L)$ and the measured $\phi_{t,ex}(f)$ total phase of the two mirrors are compared. As can be seen from the plot, the predicted phase values are in very good agreement with the measured phase values.

Using this reflection-phase information, the frequency of a defect mode for any given separation width L can be found by solving the following equation by an iteration method.

$$f_L = \frac{c}{4\pi L} [2m\pi - \phi_{t,ex}(f_L)] \quad (2.4)$$

The defect frequency f_L can also be predicted by graphical methods. The total phase

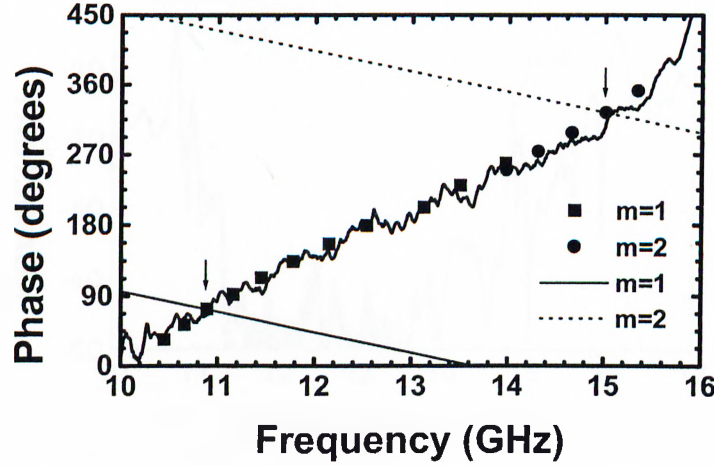


Figure 2.7: Comparison of experimental total reflection-phase contribution (thick solid line) of the walls of the cavity, with the calculated values for $m=1$ (squares) and $m=2$ (circles) for different separation widths. The plot of $\phi_t(f)$ for $m=1$ (thin solid line) and $m=2$ (dotted line) are also shown for $L=11$ mm.

of the two mirrors $\phi_{t,ex}(f)$ is plotted along with $\phi_t(f) = 2m\pi - 4\pi L \frac{f}{c}$ as a function of f . The defect frequency f_L for the chosen length L can be found from the intersection points of these two plots. As an example, the defect frequency predicted for $L=11$ mm, is shown in figure 2.7. The plot of $\phi_t(f)$ is made for $m=1$ (thin solid line) and $m=2$ (dotted line), and these two lines intersect with the $\phi_{t,ex}(f)$ at two frequencies (indicated by arrows in the figure), which are both within the band gap. We see that the agreement between the predicted and experimental defect frequencies is very good. This graphical method also explains the double defect formation for certain cavity lengths. If one of the defect frequencies is closer to the lower band edge, say corresponding to $m=1$ mode, a second frequency satisfying the resonance condition for $m=2$ can be found. An example where double defects are observed for $L=11.5$ mm, is given in figure 2.8. The $m=1$ defect mode corresponds to 10.76 GHz, while $m=2$ mode corresponds to 14.84 GHz. As the separation is further increased, modes corresponding to $m=3,4,5,\dots$ may also be observed.

Although small in size, there are extra defect modes that does not seem to fit to this theory for any value of m . These extra modes may be due to the oscillatory nature of the $\phi_{t,ex}(f)$, so that the resonance condition is satisfied at more than one frequency for

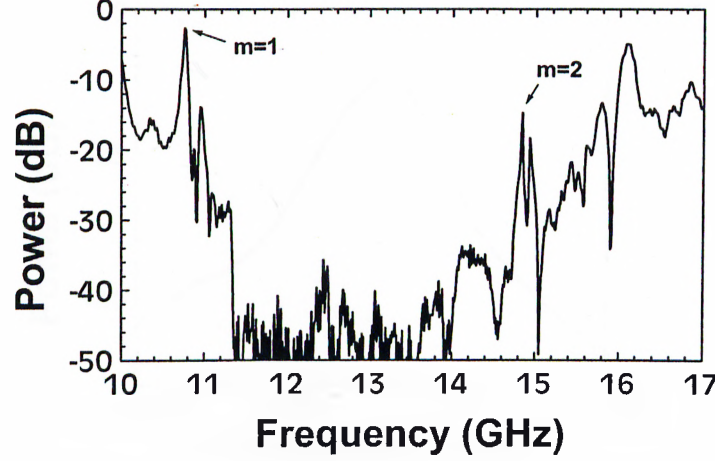


Figure 2.8: An example for double defect formation, where the resonance condition is satisfied for two separate frequencies.

a single mode, say $m=1$. In other words, graphically, there are more than one point that the expectation line $\phi_t(f)$ cuts the $\phi_{t,ex}(f)$ for a given m value. Another reason for multimode formation can be the occurrence of secondary resonances, or splittings. This may happen due to the misalignment of the mirrors with respect to each other, and due to the surface roughness of the photonic crystals. These effects may explain the situation, but later experiments done by metallic structures brought some different explanations, which would be discussed in chapter 6.

2.3 Quality Factor

The localization in the cavity obtained in this way can be quite high. The transmission spectra for such a defect where the separation length is 4.6 mm is given in figure 2.9 in an expanded frequency scale. The quality factor of the peak is found to be around 5300, which is the highest value obtained up to now for such a 3-D photonic crystal structure.

A simple approach to relate the quality factors of the defect modes to the reflectivities of the mirrors can be derived by using the Fabry-Perot resonator analogy. If we calculate

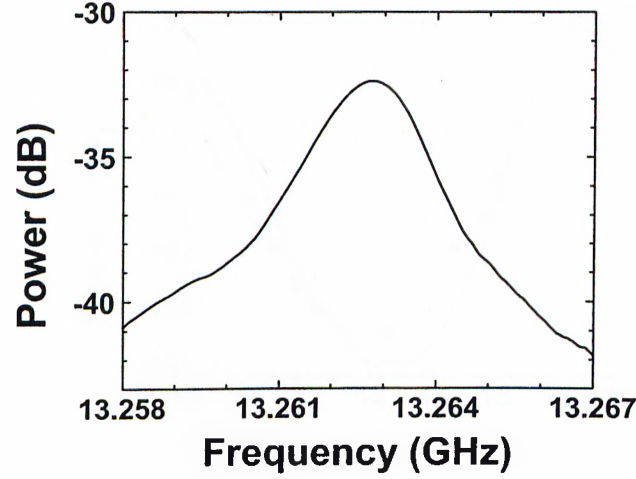


Figure 2.9: Expanded frequency scale for the defect mode, which has a Q factor of 5300.

the square of the field, which is proportional to power:

$$\begin{aligned}
 E_c \cdot (E_c^*) &= \left| \frac{j E_i t_1}{1 - r_1 r_2 e^{-j2\theta}} \right|^2 \\
 &= \frac{E_i^2 t_1^2}{(1 - r_1 r_2)^2 + 4 r_1 r_2 \sin^2 \theta}
 \end{aligned} \tag{2.5}$$

where $\theta = \beta L + \phi_t(f)/2$. The magnitude of the field drops to its half value at

$$\sin^2 \theta_{1/2} = \frac{(1 - r_1 r_2)^2}{4 r_1 r_2}$$

When the resonance condition is satisfied, θ will be close to $q\pi$ radians, that is $\theta \simeq q\pi + \theta_{1/2}$. So full width at half maximum for θ can be written as

$$2\theta_{1/2} = \Delta\theta_{1/2} = \frac{1 - r_1 r_2}{\sqrt{r_1 r_2}} \tag{2.6}$$

This is the condition where the peak drops to its half value. The sharpness of the peak is defined with the quality factor (Q) of that peak, which is the ratio of the frequency of the defect to the full width at half maximum:

$$Q = \frac{f}{\Delta f_{1/2}} \tag{2.7}$$

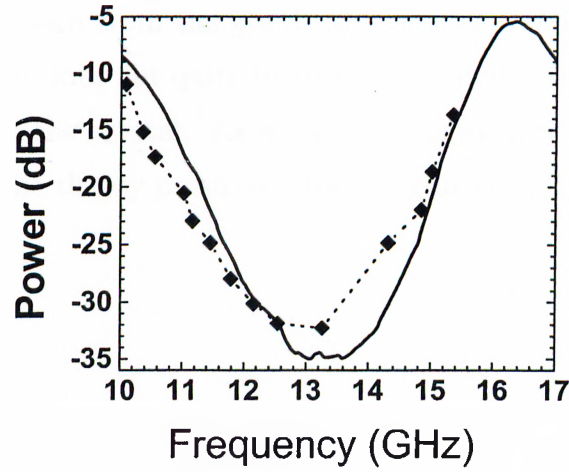


Figure 2.10: The comparison of inverse of Q values (diamonds) with the corresponding 8 layer transmission (thick solid line).

Assuming linear dependence of $\phi_t(f)$ on f with a constant α , that is letting $\phi_t(f) = \alpha f$ within the band gap, we can relate $\Delta\theta_{1/2}$ to $\Delta f_{1/2}$ as:

$$\Delta f_{1/2} = \left(\frac{2\pi d}{c} + \frac{\alpha}{2} \right)^{-1} \Delta\theta_{1/2} \quad (2.8)$$

and with this formalism, f can be written from the resonance condition as:

$$f = m\pi \left(\frac{2\pi d}{c} + \frac{\alpha}{2} \right)^{-1} \quad (2.9)$$

So the quality factor Q value can be calculated from the equation 2.7 as:

$$Q = \frac{m\pi}{\Delta\theta_{1/2}} = m\pi \frac{\sqrt[4]{R_1 R_2}}{1 - \sqrt{R_1 R_2}} \quad (2.10)$$

where we defined the reflectivities of the mirrors as $R_1 = r_1^2$ and $R_2 = r_2^2$. In our case, where $R_1 = R_2 = R$, and the transmittances $T_1 = T_2 = T = 1 - R$ are all equal, we may simplify the Q value to:

$$Q = m\pi \frac{\sqrt{R}}{1 - R} = \frac{m\pi}{T} \quad (2.11)$$

with the assumption that reflectance R is nearly unity inside the stop band. Using this information, a comparison of the Q value, with the transmittance obtained from one wall of the cavity (which is 8 layers), is made. Figure 2.10 shows the transmittance of

8 layers (solid line), and $m\pi/Q$ as a function of frequency of the corresponding defect (diamonds). As can be seen from the graph, the general trend of the plots are similar, however, the experiment does not quite fit to theory quantitatively. The reason may be due to the finite size of the crystal. As we are not using very long rods, the field may not be as localized as the theory presumes, resulting in lower Q factors.

Chapter 3

Resonant Cavity Enhanced Detectors

The fields within the cavities like Fabry-Perot resonators are usually enhanced.³⁷ This effect has already been used in optoelectronics to achieve novel devices such as resonant cavity enhanced (RCE) photodetectors and light emitting diodes.³⁸ The device within the cavity benefits from the wavelength selectivity and the large increase of the resonant optical field introduced by the cavity. In this chapter, we demonstrate the RCE effect by placing microwave detectors within the localized modes of photonic crystal defect structures.¹³ The experimental results agree well with the predictions of our model.

3.1 Detector inside planar cavity of photonic crystal

A square law microwave detector was placed inside the defect volume of the layer-by-layer dielectric photonic crystal, along with a monopole antenna. The monopole antenna was kept parallel to the polarization vector \mathbf{e} of the incident EM wave in all measurements. The dc voltage on the microwave detector was used to measure the power of the EM field within the cavity. We also measured the enhanced field by feeding the output of the monopole antenna into the input port of the network analyzer. The monopole antenna was constructed by removing the shield around one end of a microwave coaxial cable.

The exposed center conductor which also acted as the receiver, was 2 mm long. The calibrated enhancement measurements were performed in the following manner. We first measured the enhanced EM field by the probe inside the cavity. While keeping the position of the probe fixed, we removed the crystal and repeated the same measurement. This single pass absorption data of the probe was then used for calibration of the first measurement.

We first investigated the planar defect structure we have described in the previous chapter. Figure 3.1 shows the enhancement characteristics of a planar defect structure with a separation width of 8.5 mm. The measurement was done by the network analyzer and the frequency was chosen to cover the photonic band gap of our crystal. We observed a power enhancement factor of 1600 at a defect frequency of 11.68 GHz. The Q factor was measured to be 900. We then measured the enhancement characteristics of the same defect structure with a microwave detector inserted inside the same cavity (Fig. 3.2). An enhancement factor of 450 along with a Q factor of 1100, were observed at the same defect frequency.

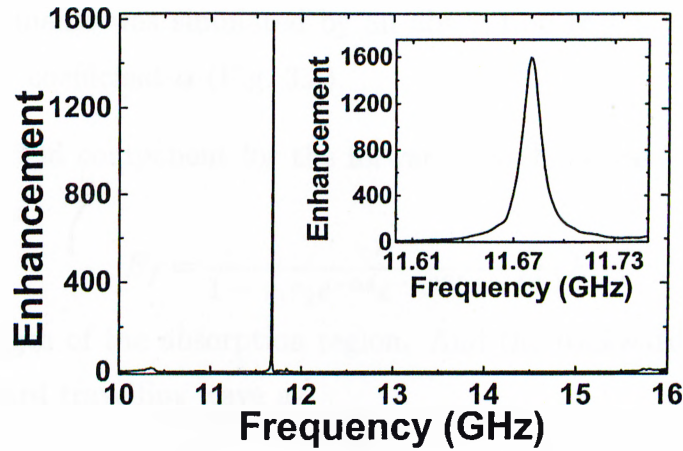


Figure 3.1: Experimental enhancement factor obtained for planar defect structure using network analyzer.

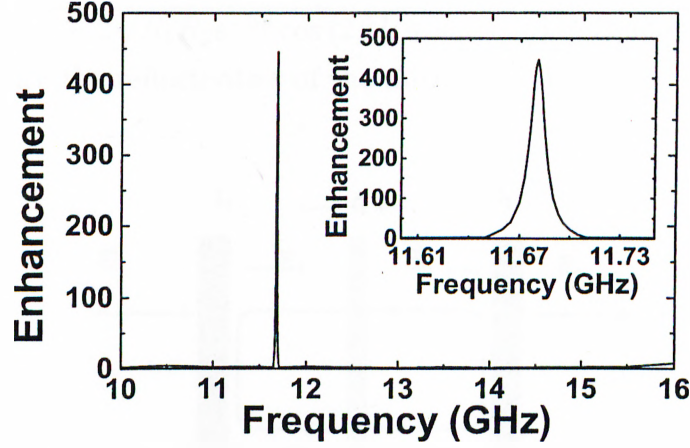


Figure 3.2: Experimental enhancement factor obtained for planar defect structure using microwave detector.

3.2 Fabry-Perot model

The discrepancy between two measured enhancement factors can be explained by modeling our structure as a Fabry-Perot cavity.³⁸ The crystals on each side of the cavity are considered as the photonic mirrors of the Fabry-Perot cavity. The probe we used in our experiments was simulated by an absorption region of thickness d , with a relative absorption coefficient α (Fig. 3.3).

The electrical field component for the forward travelling wave E_i can be related to the incident field as:

$$E_f = \frac{t_1}{1 - r_1 r_2 e^{-\alpha d} e^{-j(2\beta L + \phi_1 + \phi_2)}} E_i \quad (3.1)$$

where d is the length of the absorption region. And the backward travelling wave can be related to forward travelling wave as:

$$E_b = r_2 e^{-\alpha d/2} e^{-j(\beta L + \phi_2)} E_f \quad (3.2)$$

Using the equations 3.1 and 3.2, we can write the power enhancement factor η , which is defined as the ratio of the stored power inside the absorption layer, to the incident EM wave,

$$\eta = \frac{(1 + R_2 e^{-\alpha d})(1 - R_1)}{1 - 2\sqrt{R_1 R_2} e^{-\alpha d} \cos(2\beta L + \phi_1 + \phi_2) + R_1 R_2 e^{-2\alpha d}}, \quad (3.3)$$

where R_1 and R_2 are the reflectivities of the mirrors of the cavity.

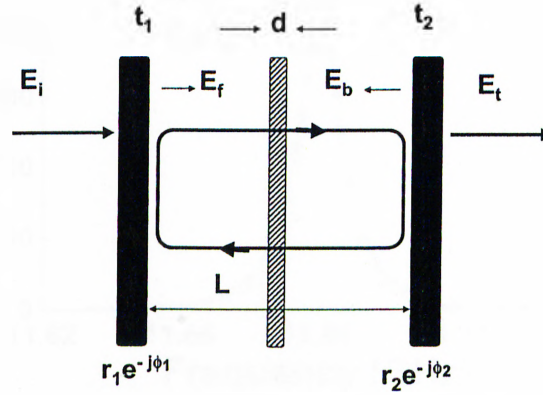


Figure 3.3: Schematics of the Fabry-Perot cavity model with an absorption region of thickness d .

The above result is normalized with respect to the incident field absorbed by the detector in the absence of the crystal. The aforementioned planar defect structure have symmetric mirrors where $R = R_1 = R_2$. We used the measured transmission characteristics to obtain the reflectivities of our photonic mirrors. As the rods are made of high quality alumina with a very low absorption coefficient, the absorption in the crystal can be neglected.³⁶ At the defect frequency, the transmission of an 8-layer crystal was 30 dB below the incident EM wave. The reflectivity of the photonic mirrors was then obtained as $R = 1 - T = 0.999$. The ideal case which maximizes η corresponds to $\alpha d = 0$, which gives a maximum enhancement factor of 2000. We then varied αd to obtain enhancement factors closer to our experimental measurements. For $\alpha d = 0.0001$, Eq. 3.3 yields an enhancement factor of 1600 (which corresponds to the value obtained from the network analyzer), while $\alpha d = 0.0011$ results in an enhancement factor of 450 (microwave detector). The increased absorption factor for the detector measurement can be explained by the relatively large volume size of the microwave detector compared to monopole antenna alone. Figure 3.4 compares the measured (solid line) and simulated (dotted line) enhancements obtained for the RCE microwave detector within the planar

defect structure. The theoretical Q-factor (1500) is comparable with the experimental Q-factor (1100).

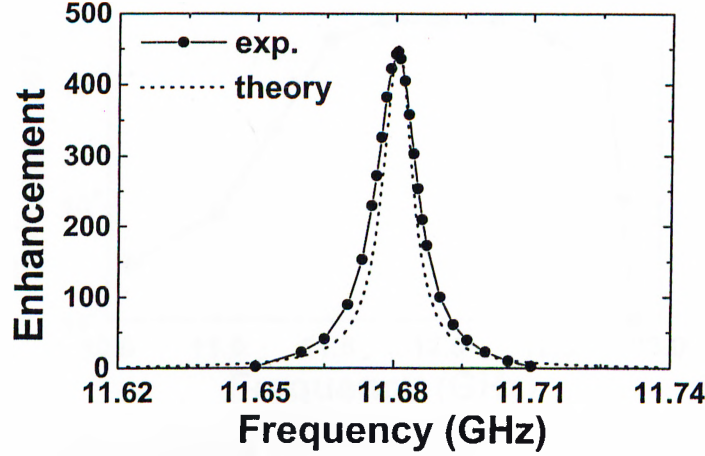


Figure 3.4: Comparison of the experimental (solid line) and theoretical (dotted line) enhancement factors for the detector inside planar cavity.

3.3 Tuning bandwidth

Fabry-Perot model suggests that η is maximized for the matching case $R_1 = R_2 e^{-2\alpha d}$.³⁸ To increase the enhancement, we increased R_2 by adding one more unit cell (4 layers) to the mirror at the back. This resulted in an asymmetric planar cavity with a 2 unit cell thick front mirror, and a 3 unit cell thick back mirror. By varying the width of the planar cavity, we measured the enhancement factors at different resonant frequencies. As shown in Fig. 3.5, the tuning bandwidth of the RCE detector extends from 10.5 GHz to 12.8 GHz. This tuning bandwidth of the RCE detector is in good agreement with the full photonic band gap (10.6-12.7 GHz) of the crystal.³⁶ As expected, the measured enhancement factors are relatively higher when compared with the symmetrical defect case. The maximum enhancement was measured to be 3450 at a defect frequency of 11.75 GHz. The theory predicted enhancement factors around 5500, which is higher than the measured values. The discrepancy can be explained by the finite size of the

photonic crystal, which limits the power enhancement of the field within the cavity.

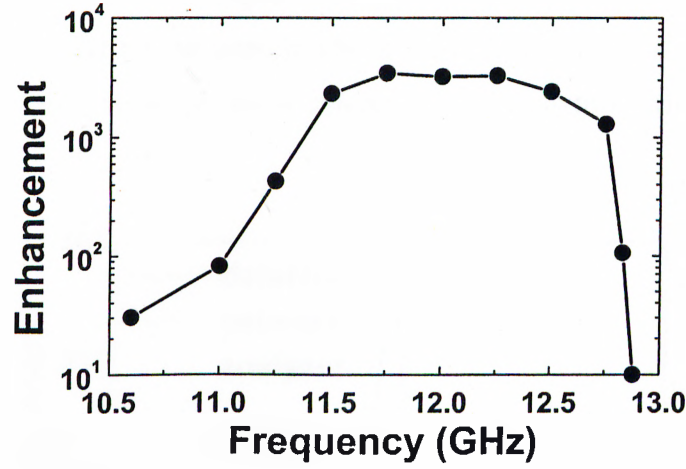


Figure 3.5: The power enhancement can be obtained at different frequencies within the band gap by changing the width of the cavity.

3.4 Box-like cavity

In order to obtain a defect that is localized in three dimensions, we modified a 16 layer crystal structure in the following manner. Part of the rods on the 8th and 9th layers were removed to obtain a rectangular prism-like cavity. The dimensions of the cavity was $4a \times 4a \times 2d$, where $a = 1.12$ cm was the center to center distance between parallel rods, and $d = 0.32$ cm was the thickness of the alumina rods. We measured the power enhancement characteristics of this structure using the method described earlier. Figure 3.6 (dotted line) shows the measurement made by the network analyzer. An enhancement factor of 290, and a Q factor of 540 were measured at a defect frequency of 12.32 GHz. We then used a microwave detector within the cavity to probe the EM field inside the localized defect. As shown in Figure 3.6 (solid line), the maximum enhancement (245) occurred at the same frequency, along with a Q factor of 680. Both measurements clearly indicate the resonant cavity enhancement for the localized defect.

Although the one dimensional Fabry-Perot cavity model will be a crude approximation for such three dimensional structures, the reduced power enhancement (along the stacking direction) can still be explained by this simple model. The photonic mirrors of the box-like defect structure were made of 7-layers (instead of 8). In contrast to the planar defect structure, these photonic mirrors were not symmetric. For the first mirror,

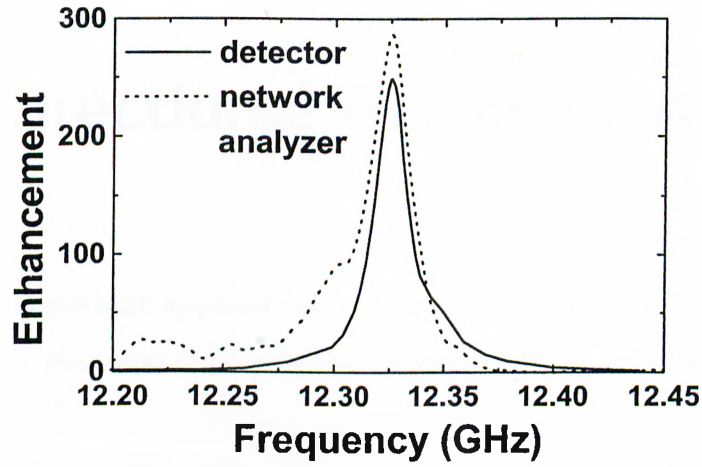


Figure 3.6: Enhancement characteristics of the box like cavity.

the polarization vector \mathbf{e} was perpendicular to the rods of the first and seventh layers. On the other hand, the polarization vector \mathbf{e} was parallel to the first and seventh layers of the second mirror. This brought an asymmetry to the reflectivities of each mirror, where we measured $R_1 = 0.978$ and $R_2 = 0.998$ for propagation along the stacking direction. Using these reflectivity values in Eq. 3.3, we calculated an enhancement factor of 300 for the measurement made by the network analyzer (with $\alpha d = 0.0001$), and 250 for the microwave detector (with $\alpha d = 0.0011$). Both of these predicted values agree well with the experiment.

Chapter 4

Highly Directional Resonant Antennas

Among the most important applications of photonic crystals, there is a great deal of growing interest for photonic crystal-based antennas.^{9,39} In microwave and millimeter-wave integrated circuits, the control of the radiation from a dipole antenna is of great importance. In such circuits, the antenna is mounted on a semiconductor substrate, which enhances the performance and functionality of the circuit. But most of the power from the antenna on a dielectric substrate is radiated into the substrate. Standard antennas on GaAs or Si radiate only 2-3% of their power into air. If a thin substrate is used to overcome the loss due to this trapping, another problem arises. A 180° phase shift comes from the reflection at the bottom conductor, resulting the radiation to cancel out at driving point. These problems can be solved, if the antenna was to be mounted on a 3-D photonic crystal, from which the radiation will fully be reflected in all directions.

The reported experimental and theoretical studies on the antenna applications mostly made use of the total reflection property of photonic crystals. The antennas mounted on photonic crystal substrate surfaces exhibited high efficiency and directivity compared to conventional antennas on dielectric substrates.^{10,40} Although high directivities which could be achieved using array antennas on photonic crystals were suggested,⁴¹ the maximum directivity that was demonstrated by Brown and McMahon using a photonic crystal-based single dipole antenna was 10, along with a radiative gain of 8.¹⁰ Very

recently, a higher gain around 80 was reported using a 2-D photonic crystal cavity and a metallic mirror.¹⁴

In this chapter, we report a photonic crystal-based resonant antenna with a very high directivity and gain. The antenna was formed by a hybrid combination of a monopole radiation source and a cavity built around layer-by-layer photonic crystal.⁴²

4.1 Radiation patterns

We used the output port of a microwave network analyzer and a monopole antenna to obtain EM waves. The monopole antenna was constructed by removing the shield around one end of a microwave coaxial cable. The cleaved center conductor, which also acted as the radiation source, was 6 mm long. The chosen length of the monopole antenna corresponds to a quarter wavelength of EM wave at a frequency of 12.5 GHz, which is close to the adjusted resonance frequency of the cavity. Input port of the network analyzer and a standard gain horn antenna were used to receive the radiated EM field from the monopole antenna. The receiver was kept free to rotate around the antenna as shown in Fig. 4.1.

We investigated the radiation characteristics of this monopole antenna, which was inserted into the planar defect structures built around a photonic crystal that consisted of 20 layers. The planar defect was formed by separating the 8th and 9th layers of the structure. In order to suppress the radiation in the backward direction, we intentionally chose one of the crystals of the cavity to have a higher reflectivity than the front crystal. This resulted in an asymmetric planar cavity with a two unit cell (8 layers) front crystal, and a three unit cell (12 layers) back crystal. The intensity through the back crystal is ~ 18 -20 dB lower than the front crystal in the 0° direction. If a symmetric cavity was used, two directional beams would emerge in both directions.

In the H-plane measurements, the antenna and the polarization axis of the receiver horn antenna was kept vertical, and were parallel to each other at all incidence angles.

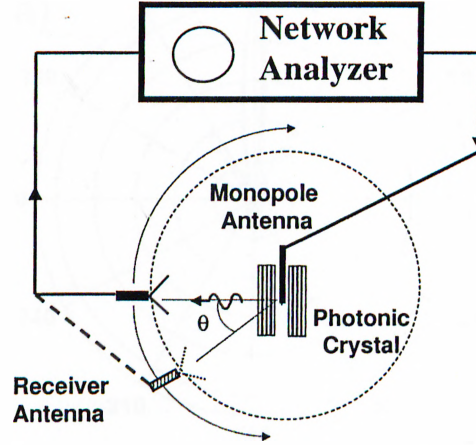


Figure 4.1: Experimental setup for measuring the radiation patterns of the monopole antenna at various angles.

We then rotated the antenna, photonic crystals and the horn antenna 90 degrees (so that the monopole antenna and the polarization axis of the horn were horizontal) to measure the radiation pattern in the perpendicular plane (E-plane). In all these measurements, the monopole antenna was kept close to the back crystal of the cavity. The antenna was parallel to the surface rods of the back crystal to maximize the directivity and the detected power.

Antenna radiation patterns were simulated by R. Biswas of ISU, with the widely used finite-difference-time-domain (FDTD) technique.³⁹ To reduce the FDTD computational space, a short dipole antenna was used in the simulations which should approximate well the monopole antenna. The time dependent Maxwell's equations were numerically integrated with the fixed frequency dipole source inside the defect volume of the photonic crystal, to obtain the far-field radiation pattern. The calculations were repeated at different frequencies of the dipole source.

We first measured the detected power at the resonance frequency of the cavity as a function of angle. Figure 4.2(a) (solid line) shows the normalized radiation pattern in H-plane, which was measured at the resonance frequency of the cavity. We observed a

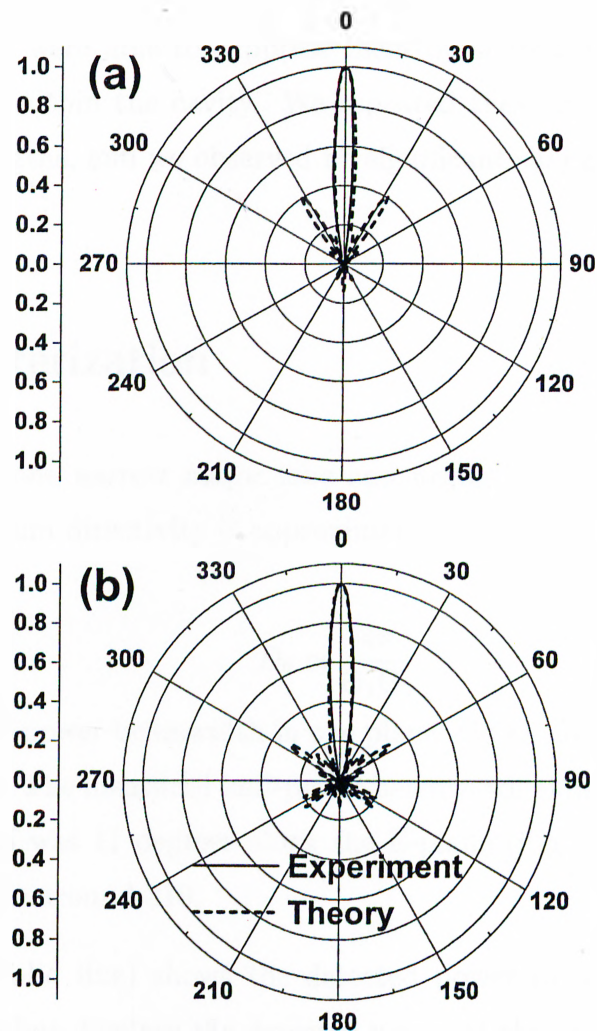


Figure 4.2: The measured (solid lines) and calculated (dotted lines) radiation patterns of the monopole antenna inside the cavity of the photonic crystal for (a) H-field and (b) E-field. The measurements and simulations were made at the resonance frequency of 11.7 GHz.

strong radiation around $\theta = 0^\circ$, where the radiation along other directions is highly suppressed. The measurements performed in the other plane (E-plane, Fig. 4.2(b), solid line) also resulted in a similar radiation pattern. The measured (solid lines) and calculated (dotted lines) radiation patterns for both planes agree well. The simulations also predict a directed radiation pattern that displays the same trends but has side lobes

other than the major lobe. We also observed such radiations along similar angles in the experiment, but we were able to suppress them by slightly varying the position of the monopole antenna within the cavity. We repeated these measurements with antennas having different lengths, and we observed no significant change in the radiation patterns for both planes.

4.2 Characterization

For antennas with one narrow major lobe and negligible minor lobes in the radiation pattern, the maximum directivity is approximately equal to⁴³

$$D_0 \simeq \frac{4\pi}{\Theta_1 \Theta_2} , \quad (4.1)$$

where Θ_1 is the half-power beamwidth in one plane and Θ_2 in the perpendicular plane to the first, in radians. The measured half-power beamwidth along the H-plane (Fig. 4.2(a)) was 12 degrees, and was 11 degrees along the E-plane (Fig. 4.2(b)). These values lead to a directivity value around 310.

Figure 4.3(a) (solid line) shows the detected power as a function of frequency at $\theta = 0^\circ$. The dotted line displays the detected power at the same angle in the absence of the photonic crystal. At resonance frequency, we observed a power enhancement factor of 180 (22.6 dB) at a defect frequency of 11.725 GHz. The radiated EM field from the monopole antenna has also frequency selectivity introduced by the cavity. The Q factor was measured to be 895.

In order to understand the effect of the resonator to the efficiency of the monopole antenna, we also measured the S-parameters of our antenna structure. Figure 4.3(b) shows the reflection power coefficient (S11) which is 30% (-5 dB) for the monopole antenna standing alone in air. This implies that the antenna radiates only 70% of the incoming power. When the antenna was inserted inside the cavity, we observed a very sharp drop (-35 dB) at resonance frequency in the reflection spectra [Fig.4.3(b), solid

line]. This drop indicates that most of the power (99.97%) is radiated out in the presence of the cavity. The maximum radiation gain for our antenna is related to the maximum directivity by $G_0 = (1 - R)(1 - A)D_0$, where R is the reflected power and A is the absorptivity of the antenna. In our case, the reflectivity at the resonance frequency is very small (0.0003). Assuming that the absorption in the antenna has a negligible value, the maximum gain has a value 300.

Such a planar cavity built around a 3-D photonic crystal should not be confused with the Fabry-Perot type of resonators that are constructed by using distributed Bragg reflectors (which are known as 1-D photonic crystals). In the former structure, the EM field is always coupled to the evanescent defect mode within the band gap irrespective of the incidence angle. However, the resonant frequency shifts as the angle of incidence of the EM wave changes in the latter case.^{43,44} It is obvious that for planar waves, 3-D and 1-D resonant structures will result in similar enhancements and directivities. In our case, the monopole antenna radiates in all directions, and all the power radiated is coupled to the evanescent mode of the defect, regardless of the direction. This is the reason we have an antenna with a very high efficiency [see Fig.4.3(b)]. However, for a 1-D structure, the radiated EM field, except a certain direction, will not be coupled to the corresponding resonant mode of the cavity.

Although our structure is suitable for narrow bandwidth applications, one can tune the defect frequency to any desired value by adjusting the width of the cavity. We observed that the resonance frequency could be tuned within a frequency range extending from 10.6 to 12.8 GHz, which corresponds to the full band gap of our photonic crystal. The directivity drops to values around 100 at the band edges, and reaches a peak value of 310 at 11.7 GHz.

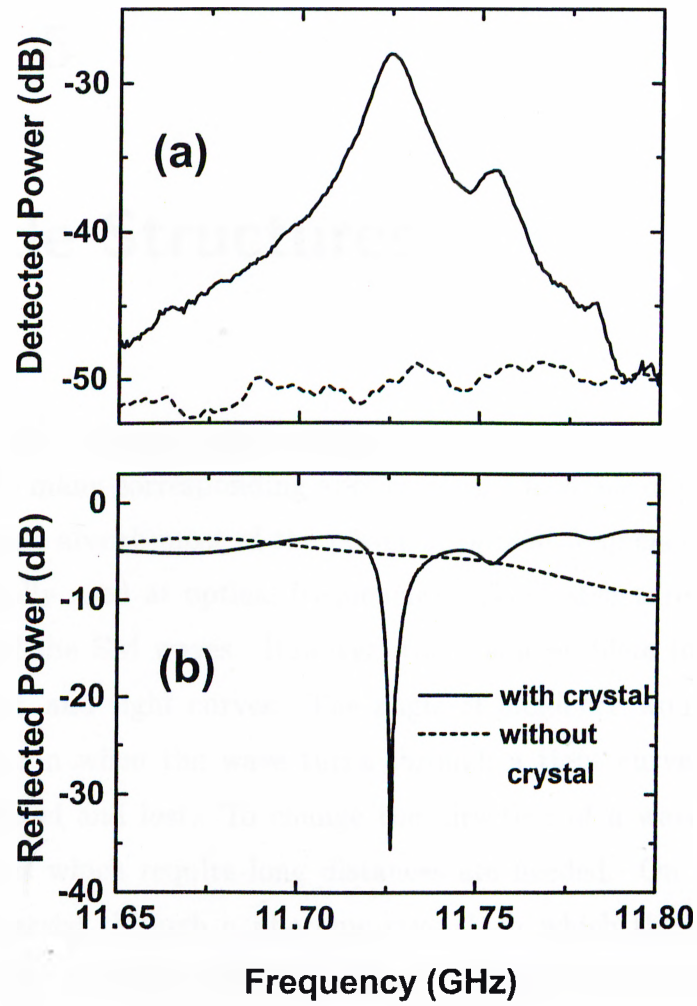


Figure 4.3: (a) Detected power of the monopole antenna with (solid line) and without (dashed line) photonic crystal around resonance frequency at $\theta = 0^\circ$. (b) The reflection power coefficient (S_{11}) measured with (solid line) and without (dashed line) photonic crystal.

Chapter 5

Waveguide Structures

Waveguides allow only certain electromagnetic wave modes to propagate inside the structure. There are many corresponding applications, which are of great importance in technology. As metals absorb most of the power at optical frequencies, dielectric-based waveguides are usually used at optical frequencies. These structures rely on the total internal reflection of the EM waves. However, there is a problem in guiding the wave through sharp edges, and tight curves. The angle of incidence would be too high for total internal reflection when the wave turns through a tight curve. So, most of the field would be radiated and lost. To change the direction of a wave with a dielectric guide, smooth curves which require long distances are needed. On the other hand, a waveguide can be carved through a photonic crystal, in which the guided modes can travel freely (Fig. 5.1). Therefore the trapped wave is guided without loss through the carved waveguide, even if it has tight corners.^{19,45–47} This would be helpful in lowering the size of integrated optical circuits. We will present our experimental results where we have observed waveguiding in photonic crystal structures.¹⁵ The dispersion diagrams calculated using the waveguide model we constructed agree well with the experimental results.

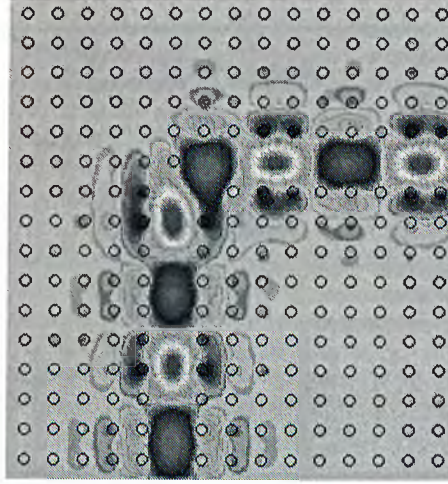


Figure 5.1: It is possible to create waveguides that permit 90° bends with 100% transmission using photonic crystals.¹⁹

5.1 Through waveguide

Figure 5.2 shows the schematics of the measurement set up that was used in our experiments. We measured the transmission-phase and transmission-amplitude properties of the two different waveguide structures, namely a parallel-plate and an L-shaped. We constructed the parallel-plate type waveguide by using two separate 3 unit cell thick layer-by-layer photonic crystals. The crystals were brought together along the stacking direction with a separation width d between them, while keeping a mirror type of symmetry between the rods of the two crystals (see Fig. 5.2). For the planar defect structure we have investigated in the previous chapters, the propagation direction of the EM wave was perpendicular to the plane of the cavity. If the propagation direction is chosen to be parallel to the plane of the cavity, the structure will have the geometry of a parallel-plate waveguide. We expect the wave to be guided through the introduced air gap, starting from a cut-off frequency which depends on the width of the gap. The guiding is limited with the full band gap frequency range of the photonic crystal, for which the crystal has the property of reflecting the EM waves in all directions.

We tested this waveguiding argument, by measuring the transmission properties

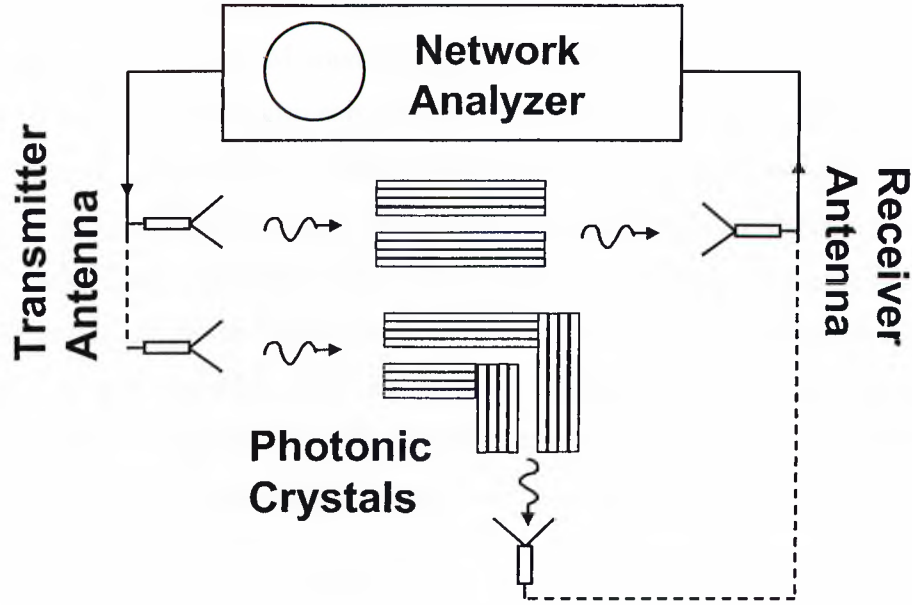


Figure 5.2: Experimental setup used to investigate the parallel-plate (upper case) and L-shaped (lower case) waveguide structures.

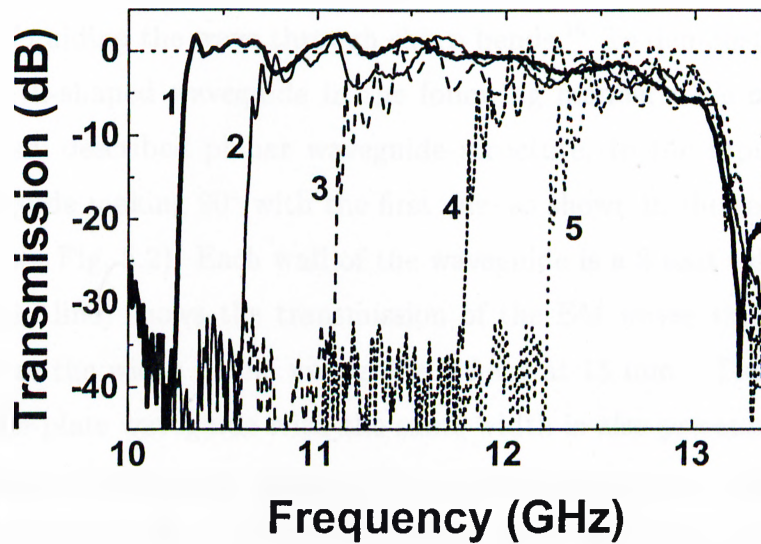


Figure 5.3: Transmission amplitude measured from parallel-plate waveguides as the separation width of the waveguide is changed. The numbers given in the plot are assigned to width of the guides as (1) 18, (2) 16, (3) 14, (4) 12, (5) 10.5 mm.

of these structures along the plane of the cavity. Figure 5.3 shows the transmission properties of the waveguide structure for different separation widths. We observed full transmission (100%) of the EM waves along a certain frequency range. The waveguiding was first observed at a minimum separation width around 10 mm, and the cut-off shifted to lower frequency values as the width of the air gap was increased. Independent of the width of the cavity, the guiding was observed to vanish at a fixed upper cut-off frequency (13.2 GHz), which corresponds to the upper band-edge of the photonic band gap. This is along our expectations as the crystals do not act as mirrors (in all directions) beyond the full band gap frequencies. The lower cut-off frequency is determined by the width of the cavity and corresponds to the resonant frequency of the Fabry-Perot resonator. This resonant frequency can easily be predicted by a Fabry-Perot defect model we have used in chapter 2.³⁶

5.2 L-shaped waveguide

As we have pointed earlier, photonic crystal based waveguides were predicted to have the property of guiding the wave through sharp bends.¹⁹ To demonstrate this effect, we constructed an L-shaped waveguide in the following manner. We coupled the output of the previously described planar waveguide structure, to the input of an other but identical waveguide making 90° with the first one, as shown in the second configuration of the set-up (see Fig. 5.2). Each wall of the waveguide is a 2 unit cell photonic crystal. Figure 5.4 (solid line) shows the transmission of the EM waves through the L-shaped waveguide where the width of the waveguide is kept at 15 mm. The transmission of a through parallel-plate waveguide with the same width is also presented (dotted line) in order to compare the frequency range of the guided wave, which agrees well with that of the L-shaped waveguide. Figure 5.5 (thick solid line) shows the transmission of the EM waves through the L-shaped waveguide. This time, the width of the cavity is kept at a value of 20 mm, for which the frequency range of the waveguide will overlap with the full band gap of the crystals. The maximum magnitude of the transmitted

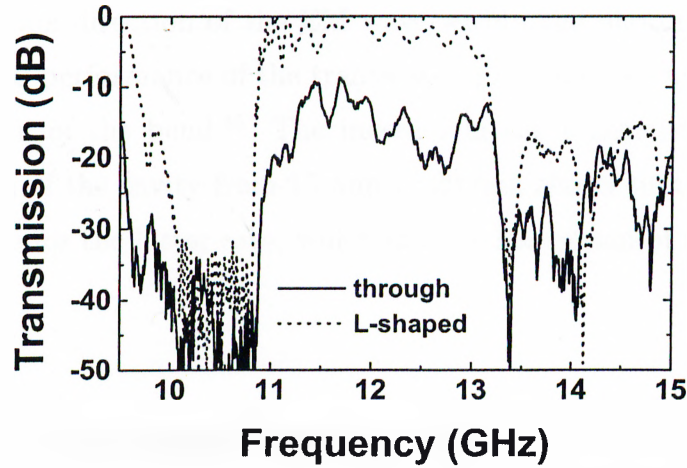


Figure 5.4: Transmission through L-shaped (solid line) and through (dotted line) waveguides.

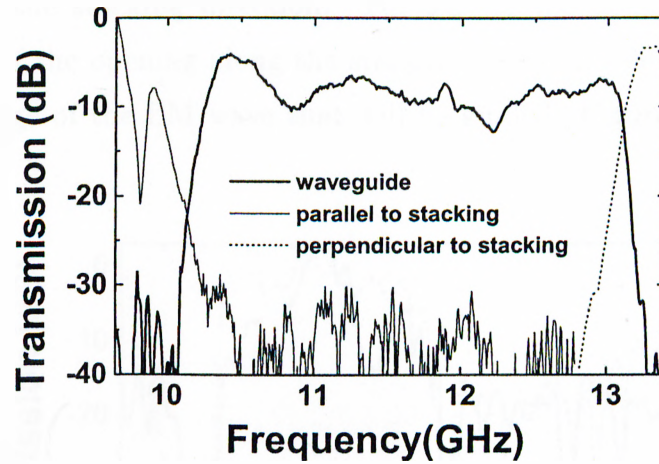


Figure 5.5: Transmission characteristics of the L-shaped waveguide of 20 mm width (thick solid line) and the transmission through the perfect crystal along stacking direction (thin solid line) and perpendicular to stacking direction (dotted line).

signal was 35% of the incident signal. The exchange of the receiver and transmitter antennas did not affect the transmission characteristics. In order to illustrate the 3D band gap, the transmission through a 4 unit cell crystal along the stacking direction (thin solid line describing the lower band edge) and the transmission perpendicular to the stacking direction (dotted line describing the upper band edge) are also shown in

Fig. 5.5. These propagation direction for the band gaps were chosen such that it matches with the propagation direction of the EM wave within the photonic crystal waveguide. The relatively poor performance of the transmission magnitude can be further increased by a proper design of the bend.⁴⁵ The increase in the transmission amplitude as we increase the width of the cavity from 15 mm to 20 mm shows that more field is coupled into the waveguide for the latter case, which may be the reason of the poor performance of the waveguide.

5.3 Two-dimensional waveguide

We constructed a 2D waveguide carved all through an otherwise perfect crystal. The wave is expected to travel through this 2D prism like opening all through the crystal perpendicular to the stacking direction. The size of the opening was 15 mm by 44 mm. The width of the opening along the stacking direction was expected to determine the frequency range of the EM wave that will be guided. Figure 5.6 (solid line) shows

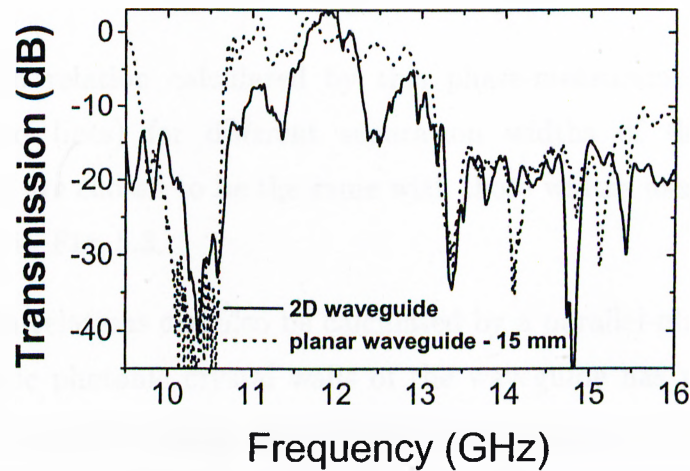


Figure 5.6: Transmission through a two dimensional waveguide(solid line), compared with the transmission through a planar waveguide with separation of 15 mm.

the transmission through this waveguide. The frequency range of the guided EM wave matches with the guided EM wave's frequency range of the planar waveguide having 15

mm width. Though full transmission is observed for certain frequencies, there are also frequencies where the amplitude of the guided wave drops to very low values (around 5% of the incident EM wave).

These results show that photonic crystals can be used for various waveguide configurations.

5.4 Dispersion diagrams

We investigated the dispersion characteristics of the planar waveguide by measuring the phase difference of the transmitted wave introduced by the guide. This phase difference, ϕ_{trans} , can be written as $\phi_{\text{trans}} = kL - k_z L$, where $k = 2\pi f/c$ is the free space wavevector, k_z is the component of the wavevector along the waveguide (see Fig. 5.7), and L is the length of the waveguide. This can be used to find the normalized propagation constant, k_z/k , as a function of frequency,

$$\frac{k_z}{k} = 1 - \frac{\phi_{\text{trans}}}{kL} = 1 - \frac{\phi_{\text{trans}} c}{2\pi f L} \quad (5.1)$$

The dispersion relation calculated by this phase-measurement method is shown in Fig. 5.8 (solid lines) for different separation widths of the waveguide. The separation widths are chosen to be the same with those widths used in the transmission measurements as in Fig. 5.3.

The dispersion relations can also be calculated by a parallel-plate waveguide model. Since the dielectric photonic crystal walls of the waveguide has a certain penetration depth that can be calculated using the reflection-phase information from the walls of the cavity, we can define an effective width for the waveguide. This approach was previously used to investigate the defect characteristics built around dielectric (see Chapter 2) and metallic photonic crystals.^{36,48} In the calculation of this effective penetration depth, one has to consider the angle dependence of the reflection phase, since the wave is

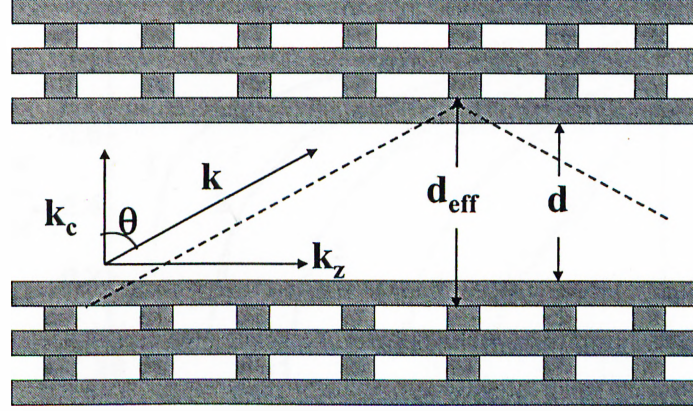


Figure 5.7: The vector diagram of the wave vector for the propagating wave inside the photonic crystal based waveguide.

considered to be bouncing between the walls of the waveguide at different angles for different frequencies. We measured the reflection phase of the EM waves from the walls of the cavity for the frequency range of the band gap, as a function of angle θ , where θ is taken to be the angle between the wavevector k and its component along the stacking direction of the crystal k_c as shown in Fig. 5.7. We calculated the effective width of the waveguide using the total phase contributions of both walls of the cavity, $\phi_{\text{ref}}(\theta, f)$,

$$d_{\text{eff}} = d + \frac{\phi_{\text{ref}}(\theta, f)}{2k}, \quad (5.2)$$

where d is the actual separation width of the waveguide. The corresponding propagation angle for each frequency is obtained from Eq. (5.1) as,

$$\theta = \arcsin\left(\frac{k_z}{k}\right) = \arcsin\left(1 - \frac{\phi_{\text{trans}}^c}{2\pi f L}\right). \quad (5.3)$$

This angle information can be used in Eq. (5.2) to find an effective width of the guide at each frequency. The k_c component of the wavevector can be calculated as $k_c = 2\pi/\lambda_c$ where $\lambda_c = 2d_{\text{eff}}$ is the cut-off wavelength of the waveguide. The dispersion relation can now be expressed as

$$\frac{k_z}{k} = \frac{\sqrt{k^2 - k_c^2}}{k}. \quad (5.4)$$

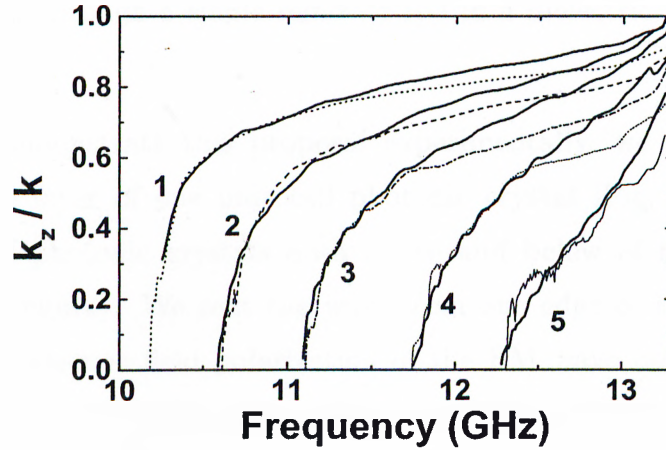


Figure 5.8: Comparison of predicted (solid lines) and theoretically calculated (dotted lines) dispersion diagrams for the waveguides with different separation widths (see Fig. 5.3).

Note that, since k_c is considered to be constant, after some frequency, the square-root becomes real, so that the waves after that cut-off frequency (defined by k_c) can propagate in the guide. For frequencies less than the cut-off frequency, k_z is imaginary, and such modes (evanescent modes) cannot propagate in the waveguide.⁴⁹ Figure 5.8 compares the parallel-plate waveguide model dispersion relations [obtained from Eq. (5.4), dotted lines] with the dispersion relations obtained from the transmission phase measurements [using Eq. (5.1), solid lines]. As can be seen from the plots, the results are in good agreement for different separation widths of the guide, except for the higher frequency regions of the waveguide. This discrepancy is mainly related to the inaccurate reflection phase information (due to experimental limitations) at higher incidence angles, $\theta > 70^\circ$.

5.5 Guided waves through removed rods

The first waveguide structure we investigated was the planar waveguide, where the EM wave is confined in only one direction. Next, we tried to introduce a waveguide which is fully confined (in two dimensions) utilizing the 3-D band-gap of the photonic crystal: the

box like opening carved within the crystal. It was previously proposed that EM waves can also be guided through a single removed rod in a dielectric layer-by-layer photonic crystal.^{50,51}

In order to demonstrate this proposal experimentally, we first removed a single rod from a single layer of one unit cell photonic crystal [Fig. 5.9(a), left side]. We placed 3 unit cell photonic crystals both above and below of this crystal (which are not shown in the figure). We sent the wave from one edge of the opening created by this removed rod, electric field polarization of the EM wave being along the stacking direction (perpendicular to the plane of the layer from which the rod was removed). We observed the formation of a waveguiding transmission band within the stop band of the photonic crystal, with very high transmission amplitudes, reaching 100% at certain regions [Fig. 5.9(a), right side]. We believe that transmissions exceeding 0 dB are due to the lens effect of the photonic crystals. By removing one more (adjacent) rod from the same layer [Fig. 5.9(b), left side], we observed that the lower cut-off frequency of the waveguiding band decreases [Fig. 5.9(b), right side]. This was expected, since the second waveguide had a wider cross-section when compared to first. We still had 100% transmission within the waveguiding band.

We then created a bend in this waveguide structure (L-shaped waveguide), by removing parts of the two rods from two adjacent layers, as shown in Fig. 5.9(c), left side. This structure was theoretically shown (by Chutinan and Noda) to guide the EM wave through the sharp bend with 100% efficiency within the full frequency range of the photonic band gap. We observed very high transmission from this structure [Fig. 5.9(c), right side], when compared to transmission amplitudes we measured from sharp bends for the planar waveguide structures. However, the frequency range of our waveguide covers only part of the photonic stop band (similar to the single rod removed results), which contradicts with the simulations (of Chutinan and Noda). The simulations made by Sigalas *et al.*, which predicts a small frequency range within the band gap for such a waveguide structure, shows a better agreement with our experimental results.⁵¹ This waveguide structure was found to be superior to the planar waveguide, considering high

transmission amplitudes measured through sharp bends.

Waveguiding through localized coupled cavities is a good example to a number of different waveguiding mechanisms which are under investigation.^{52–55}

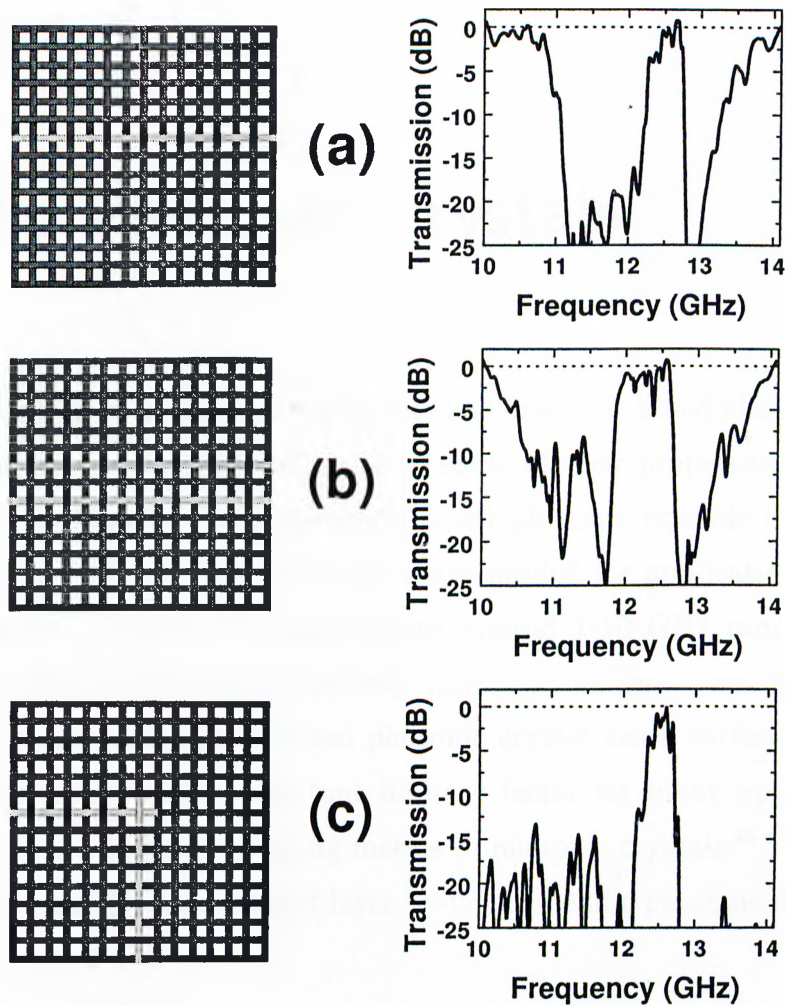


Figure 5.9: The schematics (left side) and the transmission characteristics (right side) of waveguide structures, (a) with a single missing rod, (b) with two adjacent missing rods, (c) with two crossing waveguides.

Chapter 6

Metallic Photonic Crystals

Earlier investigations were mainly concentrated on dielectric based photonic crystals, and were successful in various applications. But some of their properties restrict the wide usage of these materials. First, dielectric based photonic crystals have low rejection rates per layer, so a large number of layers are needed for applications requiring high isolation purposes. Second, for applications around 1-10 GHz range, these crystals become impractical due to their relatively large surface area. As an example, for a 2 GHz application, the dielectric based photonic crystal has a surface area larger than 1 square meter, which is an important limiting factor for many applications. These problems can be solved by introducing metals to photonic crystals.⁵⁶⁻⁵⁸ In this chapter, we will present a full investigation of layer-by-layer metallic photonic crystals.^{48,59,60}

6.1 Crystal structure

In this chapter, we have investigated the properties of two types of layer-by-layer metallic photonic crystals. The first structure, in which the stacking sequence repeats every four layers, is the equivalent of a face centered tetragonal (fct) lattice as shown in Fig. 6.1(a). Figure 6.1(b) shows the other structure similar to the first, but with a repeating sequence

of 2 layers, which is the analog of a simple tetragonal (st) lattice. The metallic rods used in these crystals were 0.8 mm wide, 2.5 mm thick, and 120 mm long, and were placed with center to center separation of 7.6 mm. The rods were obtained by machining $150 \times 150 \times 5$ mm aluminum blocks. These blocks were then stacked together to form either fct or st structures depicted in Fig. 6.1.

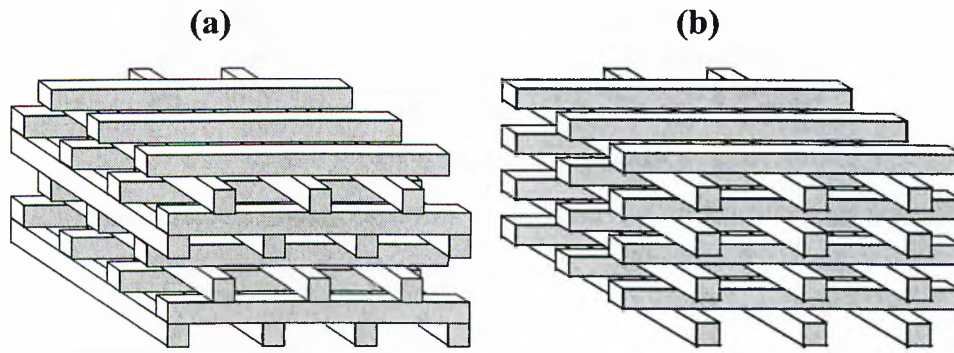


Figure 6.1: Schematics of (a) fct and (b) st based metallic photonic crystals.

6.2 Transmission properties of metallic photonic crystals

We first measured the transmission properties of both structures. Figure 6.2 compares the transmission properties of 6 layer fct and st based crystal structures where the propagation direction of the EM wave is along the stacking direction. Both crystals yielded band gaps with upper edges around 20 GHz, and no lower edge exists down to 10 GHz. Figure 6.3 shows the rejection ratios for two different crystal structures at 12 GHz, as the number of layers are increased. The typical rejection factors of 7-8 dB per layer are observed within the metallicity-gap, which is significantly superior to dielectric-based photonic crystals having a maximum rejection of 3-4 dB per layer.

For the calculations of the EM wave transmission through the photonic crystals, the transfer matrix method (TMM) introduced by Pendry and MacKinnon,⁶¹ is used. In TMM, the total volume of the photonic crystal is divided into small cells. The fields in

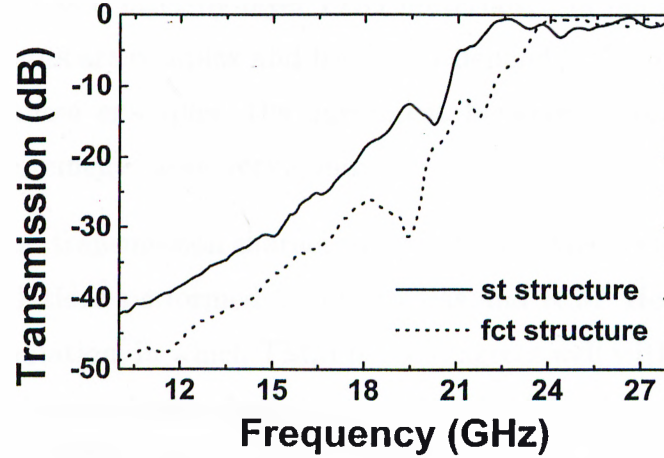


Figure 6.2: Transmission characteristics of 6 layer fct and st based metallic photonic crystals.

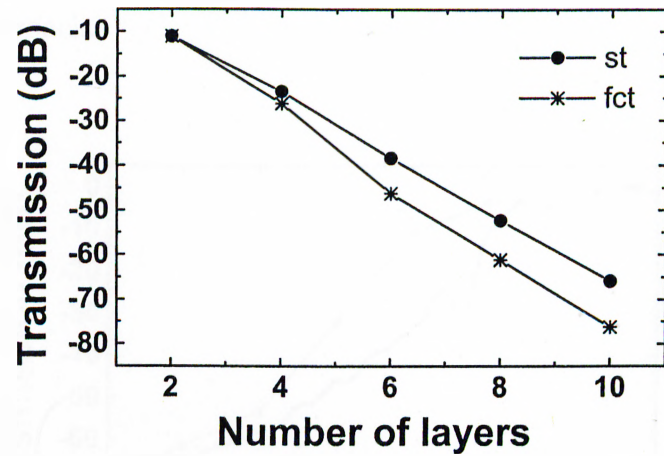


Figure 6.3: Change in the rejection rates of these crystal structures as the number of layers are increased.

each cell are coupled with those in the neighbouring cells. Then the transfer matrix can be defined by relating the incident fields on one side of the photonic crystal with the outgoing fields on the other side. Using TMM, the band structure of an infinite periodic system can be calculated. But the main advantage of TMM is for the calculation of transmission and reflection coefficients for EM waves of various frequencies incident on a finite thickness slab of the photonic crystal. In that case, the material is assumed to be periodic in the

directions parallel to the interfaces. The TMM has previously been applied in studies of defects of dielectric-based layer-by-layer PBG materials,⁶² of photonic crystals in which the dielectric constants are complex and frequency dependent,⁶³ and in metallic photonic crystals.⁵⁶ In all these examples, the agreement between theoretical predictions and experimental measurements were very good.

The experimental transmission characteristics of a ten layer crystal is compared, with the computer simulations performed by M. Sigalas and K.M. Ho of ISU, in figure 6.4. We see that the simulation, in which TMM is used, agrees well with the experiment. The band edge is located around same frequency of 20 GHz. The attenuation obtained inside the gap is around 70 dB for both results. In the computer simulations, TMM is used, where each unit cell is divided into $12 \times 12 \times 8$ cells. Although the conductivity of the metal is very high, because of convergence problems of TMM, a smaller value is chosen for the simulations. The small discrepancy between the model and the experiment may arise from this approach.

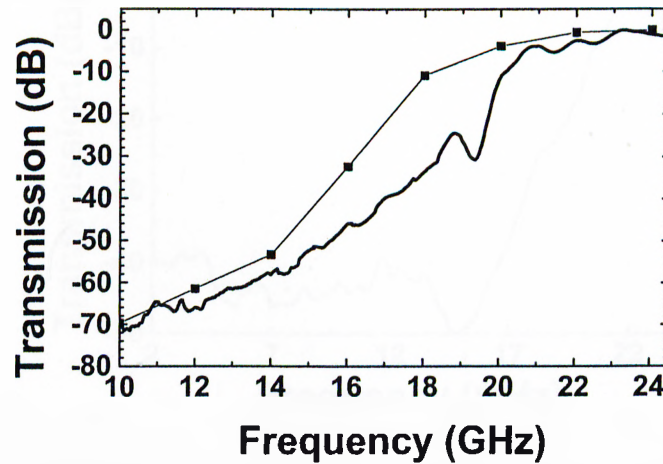


Figure 6.4: Comparison of the experimental transmission (thick solid line) of the 10-layer metallic crystal with the theoretical simulations (thin solid line).

The metallicity gap is expected to extend down to 0 GHz. In order to verify this, we measured the transmission properties of a 10 layer st based metallic crystal using two monopole antennas, instead of standard gain horn antennas. The monopole antennas,

which were constructed by removing the shield around one end of a microwave coaxial cable, were used to transmit and receive the EM wave radiation. As seen in Fig. 6.5, the band gap still exists even at frequencies as low as 2 GHz. Since the monopole antenna radiates in all directions, these measurements also reveal the fact that the metallicity gap conserves its property of reflecting the EM wave in all directions. The relatively low rejection ratio observed, which is still higher than its dielectric equivalent, is mainly due to the following two reasons: First, the finite size of our crystal compared to large wavelengths at which the measurement is made was a limiting factor. Second, the radiation efficiencies of the monopole antennas used were relatively poor. As we mentioned earlier, if dielectric materials were used, the crystal surface area should be larger than 1 square meter to have a band gap at 2 GHz. This metallic crystal we investigated, which is suitable for applications at these frequencies, has a surface area of only 225 square centimeter. The two orders of magnitude reduction in the surface area makes the usage of metallic photonic crystals feasible for low frequency applications.

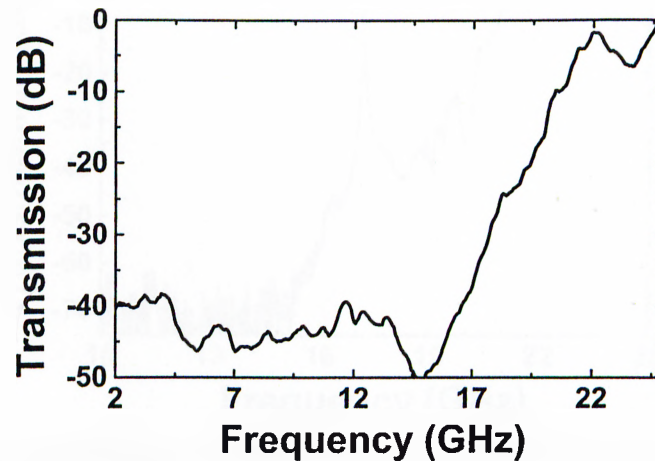


Figure 6.5: The transmission measurement performed by monopole antennas show that the metallicity gap extends down to lower frequencies.

6.3 Defect structures in metallic photonic crystals

It was previously shown in dielectric based layer-by-layer photonic crystals that defect structures around this geometry can be built by means of adding or removing rods from an otherwise perfect crystal. The same idea was used to investigate the defect characteristics of these metallic photonic crystals. Figure 6.6 shows the transmission properties of a 14 layer st type photonic crystals where the 7th layer is the defect layer with a single missing rod. The defect mode was only observed when the electric field polarization vector of the incident EM wave \mathbf{e} was parallel to the rods of the defect layer. The defect mode was observed at 17.2 GHz with a peak transmission amplitude of -7 dB, and a Q factor of 750. Increasing the number of layers to 18 (where the 9th layer was chosen as the defect layer) yielded a defect mode with an increased Q factor of 1740 and a peak transmission of -19 dB (Fig. 6.7).

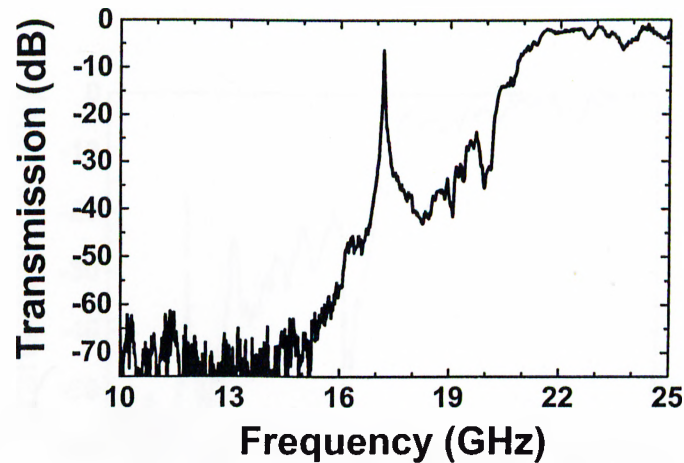


Figure 6.6: Transmission characteristics of a 14 layer st based crystal with a single rod removed defect.

A similar defect structure built around fct based photonic crystal gave a higher Q factor of 950, but with a low peak transmission amplitude of -30 dB (Fig. 6.8). This put a limit to achieve a higher Q factor by increasing the number of layers, where the peak transmission dropped below the noise level. In the following investigations, we concentrated on st based metallic photonic crystals, which are superior to fct based

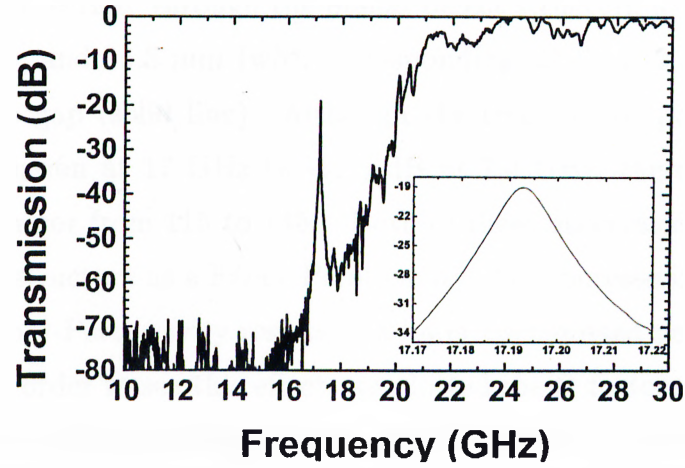


Figure 6.7: Transmission characteristics of an 18 layer st based crystal with a single rod removed defect structure.(Inset: Expanded frequency scale around resonance frequency)

photonic crystals considering the advantages of the higher peak amplitude and maximum achievable Q factors.

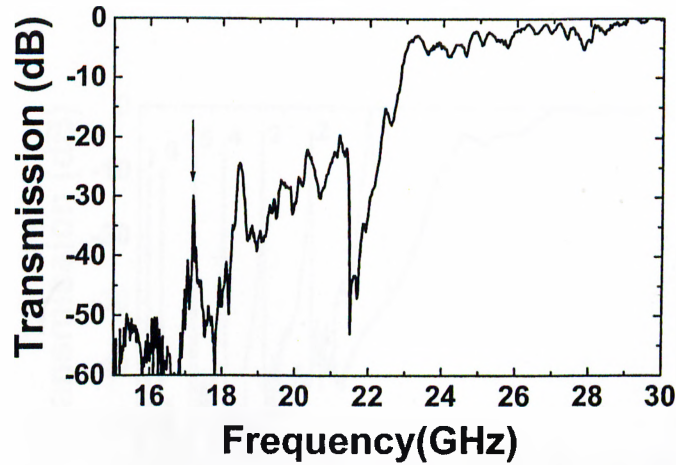


Figure 6.8: The defect characteristics of a 14 layer fct based crystal with a single rod removed defect structure.

We then investigated the planar type of defect structures, built around an 8 layer st based photonic crystal. The planar defect was obtained by separating the 4th and 5th layers of the crystal. This resulted in a planar air gap between the two photonic mirrors,

each formed of a 4 layer (2 unit cell) crystal. Figure 6.9 shows the transmitted EM wave, along the stacking direction, through the planar defect structure with separation widths of 3, 5, 7, 9, 11, 14, and 15.5 mm (with corresponding labels 1, 2, 3, 4, 5, 6, 7, dotted lines), and with no gap (solid line). Although the transmitted peak amplitude drops from 100% transmission at 17 GHz to -11.3 dB at 7.4 GHz, there exists a significant increase in the Q factor from 115 to 1450. Both of these observations can be explained by considering our structure as a Fabry-Perot cavity. The increase in the reflectivities of the mirrors of a Fabry-Perot cavity results in a lower transmitted peak amplitude, and a higher Q factor. In order to see this effect, we plotted the Q factors of the defect modes as a function of inverse transmission of the mirrors (4 layer crystal) of the cavity at the corresponding defect frequency (Fig. 6.10). The curve is expected to be linear if the mirrors of the cavity were large compared to the resonant wavelength of the cavity. As the resonant wavelength and the cavity width increases, due to finite size of our crystal mirrors, the curve deviates from linearity and flattens. These results show that this structure can be used to create defect modes with high Q factors at frequencies as low as a few GHz, which is nearly impossible for dielectric based photonic crystals.

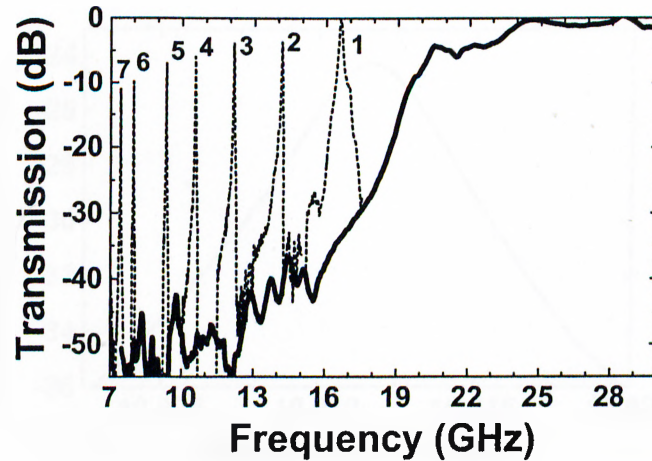


Figure 6.9: Transmission characteristics of 8 layer st based photonic crystal with no gap (solid line), and with planar defects with separation widths of (1) 3 mm, (2) 5 mm, (3) 7 mm, (4) 9 mm, (5) 11 mm, (6) 14 mm, (7) 15.5 mm (dotted lines).

Another way to increase the Q factors of these planar defect structures is to increase

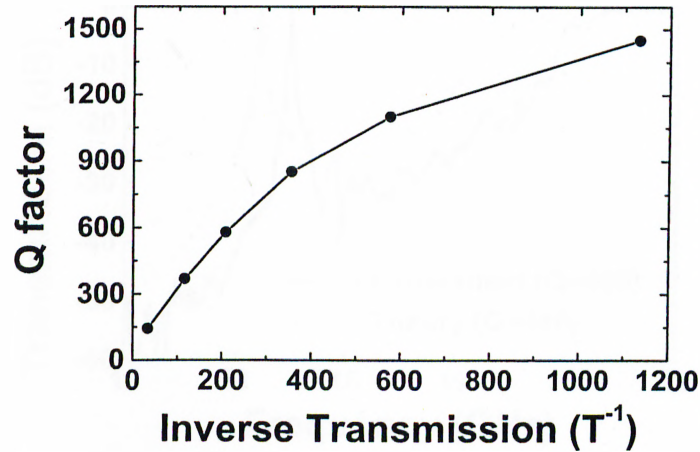


Figure 6.10: The change in the Q factor of the defect modes as a function of inverse mirror transmission of the cavity at the defect frequency.

the rejection ratio of photonic mirrors of the cavity by increasing the number of layers. As shown in Fig. 6.11, a 12 layer photonic crystal separated from the middle with a separation width of 10 nm resulted in a Q factor of 2250, with a peak transmission amplitude of -25 dB at 10.6 GHz.

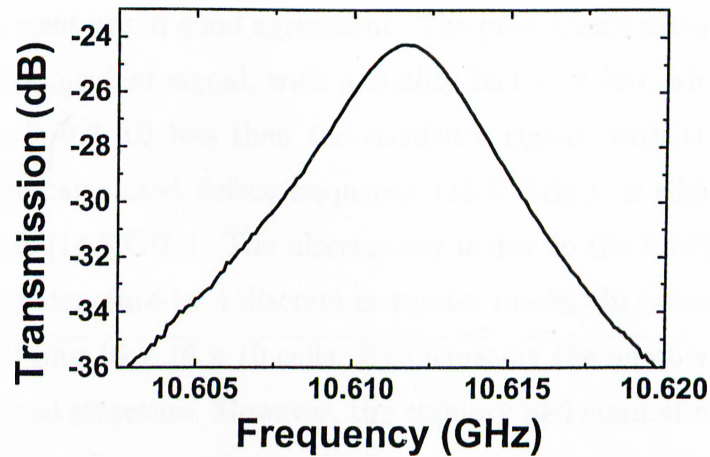


Figure 6.11: Transmission characteristics of a planar defect mode with a Q factor of 2250, in an expanded frequency scale.

The TMM requires periodicity in the directions parallel to the interfaces. For

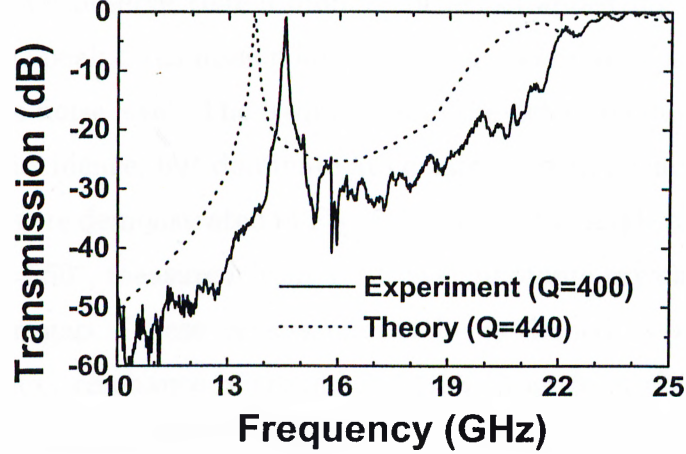


Figure 6.12: The comparison of the measured (solid line) defect characteristics of a 10 layer st based crystal with the theoretical simulations (dotted line). The defect is created by removing the fifth layer of the crystal.

comparison, we formed a planar defect by removing all the rods in a single layer. A 10-layer thick st structure where the 5th layer is chosen as the defect layer, is used for both theoretical simulations and experimental measurements. Calculations are again performed by M. Sigalas and K.M. Ho of ISU. Figure 6.12 compares the predicted theoretical transmission with the experimental results. As can be seen from the plot, theory and experiment are in good agreement. The peak transmission of the experiment is 0.9 dB below the incident signal, with a quality factor of 250, while the transmission of the simulation is 0.2 dB less than the incidence signal, with the same Q value of 250. However, the calculated defect frequency (13.7 GHz.) is slightly lower than the experimental result (14.5 GHz). The discrepancy is due to the limitations coming from simulating the real structure by a discrete computer model. In present calculations, the unit cell is divided into $16 \times 16 \times 10$ cells. By increasing the number of cells, the model gets closer to the real structure. However, the memory and computer time requirements for higher number of cells make those calculations almost impossible.

We continued to explore the properties of the planar defects in metallic structures by changing the angle of incidence of EM wave. Increasing the angle of incidence, peaks other than the main peak at $\theta = 0^\circ$ (where θ is the angle between the surface normal

of the crystal and the incident EM wave) came into view. If we continue to increase the angle further, we observe that a number of peaks appearing at higher frequencies dominate, while the peak transmission amplitudes of lower frequency modes gets smaller, disappearing at the noise level. The frequencies of the defect modes do not shift with the changing angle of incidence, but dominate at certain fixed frequencies for certain angles. These observations are demonstrated in Fig. 6.13, where the angle of incidence is changed from $\theta = 0^\circ$ to $\theta = 50^\circ$, measured from a 12 layer photonic crystal separated from the middle by a 5 mm gap. These defects cannot be explained by a simple Fabry-Perot model, since the next resonance is around 7-8 GHz away from the observed one, while the consecutive peaks appear with a separation less than 1 GHz. An explanation can be made using the theory of resonant cavities, where the reflecting mirrors are considered to be curved. The solution for this structure is a combination of Hermite Polynomials, which results in additional peaks other than the main resonance. This unexpected phenomena is under further theoretical and experimental investigation.

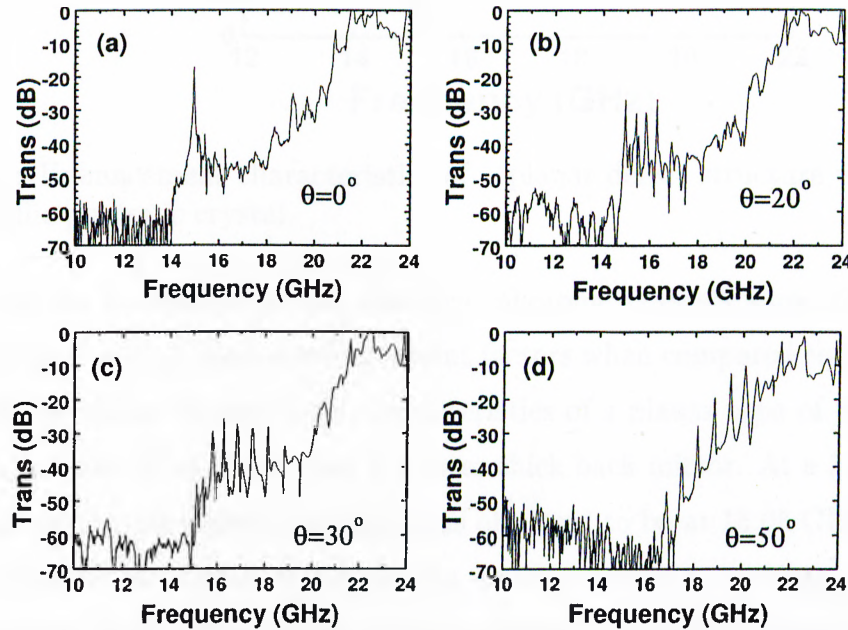


Figure 6.13: The additional defect modes observed for planar defect structures with increasing angle of incidence.

6.4 Resonant cavity enhancement

In order to demonstrate the RCE effect in metallic photonic crystals, we placed a monopole antenna inside the defect volume of planar defect structures described above. As we did in the detector measurements with the dielectric crystals, we used the network analyzer and the standard gain horn to obtain EM waves, and the monopole antenna, which is also connected to the network analyzer, as a receiver. The single pass absorption data of the probe was used to calibrate the measured enhancements.

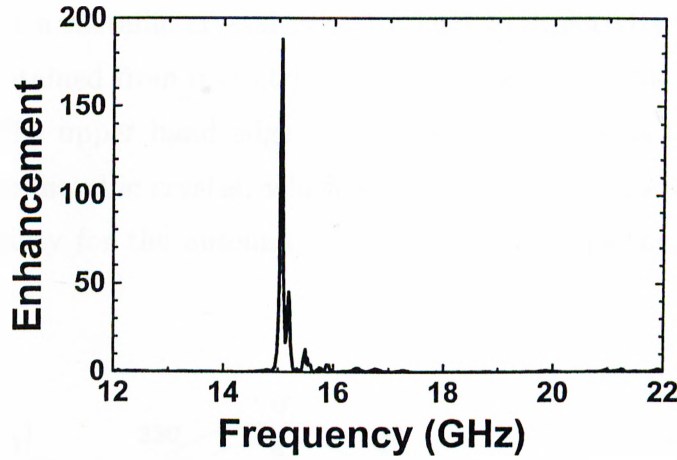


Figure 6.14: Enhancement characteristics of a planar defect structure within 8 layer st based metallic photonic crystal.

Our previous investigations on dielectric photonic crystals show that asymmetric planar cavities results in higher enhancement factors when compared to symmetric ones. Figure 6.14 shows the enhancement characteristics of a planar type of defect structure, with a 4 layer thick front mirror and a 6 layer thick back mirror. At a 5 mm separation width of the cavity, the defect frequency was observed to be at 15.08 GHz. We observed a power enhancement factor of 190 at the defect frequency, with a Q factor of 335. When compared with enhancement factors obtained in cavity structures built around dielectric photonic crystals, this value is rather small. This may be the result of small but finite absorption coefficients of metals, which exists even at microwave frequencies. This absorption becomes significant when we consider the high number of times the field

circulates inside the cavity and experiences a loss in each cycle. Still these investigations suggest the possibility of using embedded detector inside a metallic photonic crystal, as a frequency selective RCE detector, with an increased sensitivity, efficiency when compared to conventional detectors.

6.5 Directive radiation patterns from metallic photonic crystals

We have showed that a metallic crystal can also lead to directivity and gain values as high as the values obtained from dielectric photonic based resonant antennas, with less number of layers. The upper band edge of the metallic crystal is located at 20 GHz. The stop band of the metallic crystal, which extends down to zero frequencies, offers a wide range of tunability for the antenna, which is a great superiority for this type of structures.

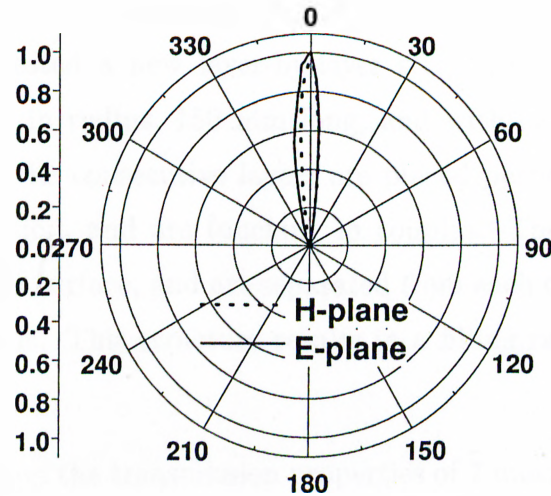


Figure 6.15: Radiation characteristics of a monopole antenna inside a planar cavity built around metallic photonic crystals.

For this metallic crystal, the planar defect was formed by separating the 4th and 5th

layers of a total 10-layer structure. This resulted in an asymmetric planar cavity with 4 layer front mirror and a 6 layer back mirror. With the 7-8 dB attenuation per layer within the metallicity gap, the additional 2 layers at the back were enough to suppress the radiation in the backward direction for this case.

Figure 6.15 shows the radiation pattern for the metallic structure at the resonant frequency of the cavity, which was adjusted to be 15 GHz. The measured half-power beamwidth along the H-plane (Fig. 6.15, dotted line) was 12 degrees, and was 13 degrees along the E-plane (Fig. 6.15, solid line). These values lead to a directivity value around 260. We observed a power enhancement factor of 200 (23 dB) at a defect frequency of 15 GHz.

6.6 Towards lower filling ratios

Although the metallic crystal we have investigated has a quite lower filling ratio (11%) when compared with its dielectric equivalent (30%), considering the high rejection ratio property of metals, it is possible to lower the filling ratio further. Therefore, we constructed and tested a new layer-by-layer structure, with cylindrical metallic rods which are 0.7 mm in radius, 150 mm long, and with center to center separation of 6 mm. The rods of the consecutive layers are placed perpendicular to each other, along the stacking direction, and are touching in couples. These touching couples of layers form a square mesh surface, and are separated from each other by 6 mm in st and 3 mm in fct based crystals. This structure results in a filling ratio of 1.1% in st and 2.2% in fct crystals.

Figure 6.16 shows the transmission properties of 7 mesh layer fct (a) and st (b) based photonic crystals. The upper band edge is at 24 GHz in fct based crystal, and shifts to 15 GHz in st based crystal. The metallicity gap extends to lower frequencies as expected. The average rejection rate per mesh layer of these crystals is around 8-10 dB, which is superior to that of the dielectric based photonic crystals.

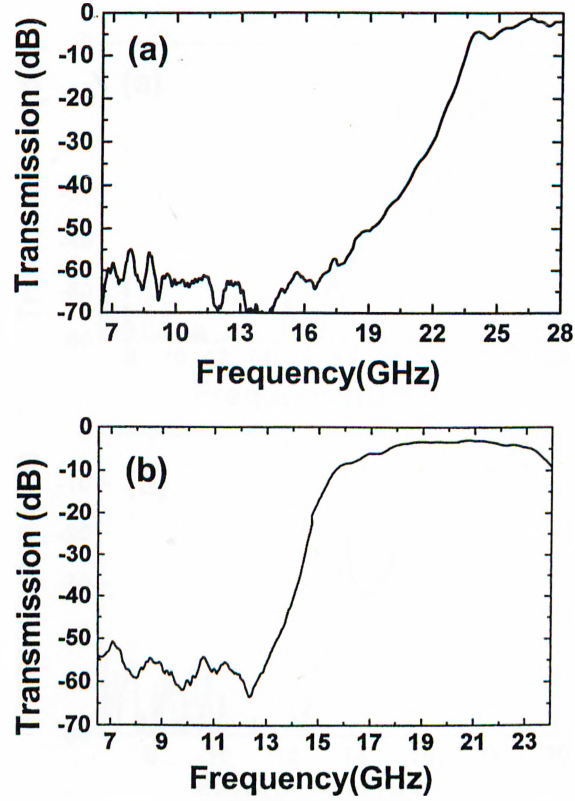


Figure 6.16: Transmission properties of low filling ratio (a) fct and (b) st based crystals.

Defects created by removing rods in this structure resulted in similar defect modes observed in other photonic crystals, but with lower peak transmission amplitudes and lower Q factors. Figure 6.17 shows the transmission properties of a 7 mesh layer fct (a) and st (b) based crystals with a defect introduced by removing a single rod from the 4th layer. This time, contradictory to the other type of crystal, fct based crystal is superior to st based one considering the higher peak transmission amplitudes (-11.2 dB in fct and -18.4 dB in st) along with same Q factors (150 in both). The relatively poor defect characteristics of st based crystals may be assigned to the leakage of the EM waves from the sides of the separation planes of the consecutive touching couples of layers, which is lower (but still significant) in fct based crystals. These results, although not as good as the previous type of crystal, is of great importance considering applications which require crystals that are light and that have low filling ratios. Also, since metals exhibit high

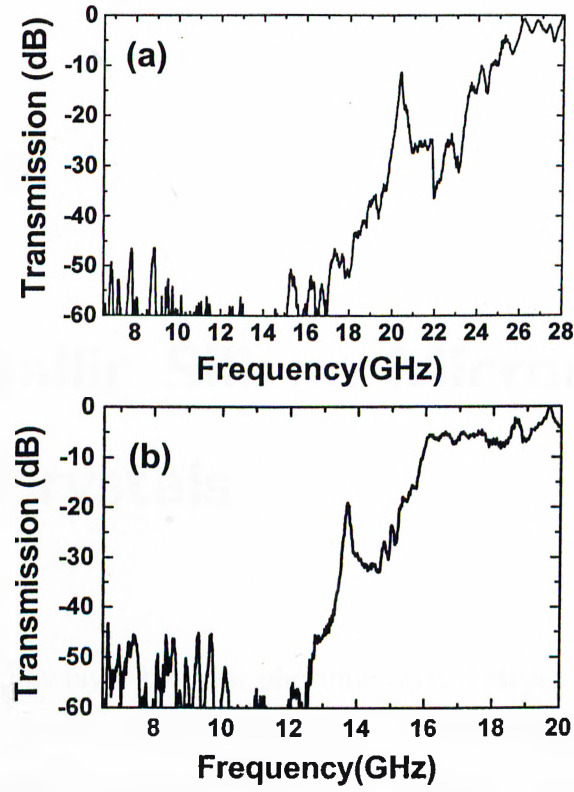


Figure 6.17: Characteristics of single rod removed defect structures built around (a) fct and (b) st based low filling ratio photonic crystals

absorption at optical frequencies, these crystals with their minimized metal contents, when compared to the other metallic crystals we investigated, will be quite useful at optical frequencies if built in sufficiently small dimensions.

Chapter 7

Quasi-Metallic Silicon Micromachined Photonic Crystals

The dielectric and metallic layer-by-layer photonic crystal structures were first fabricated at microwave frequencies.^{27,59} Various techniques have been reported for the fabrication of dielectric layer-by-layer photonic crystals at different frequency regions,^{28,30,64,65} and recently at optical frequencies.³³⁻³⁵ However, the limitations of the standard machining techniques used to fabricate 3D metallic photonic crystals restricted the experimental demonstrations and technological applications of these crystals to microwave frequencies.^{58,60,66-69} Using standard deposition techniques, one dimensional periodic metallic structures were fabricated at optical frequencies.⁷⁰ 2D metallic photonic crystals were also demonstrated to have a band gap in the THz range.⁷¹ 3D metallic structures standing on dielectric supports operating at infrared wavelengths were also demonstrated.^{72,73} However, these 3D structures do not have the advantage of a band gap extending to zero frequency due to non-touching metallic layers. The fabrication of 3D metallic photonic crystals at higher (compared to microwave) frequency regions with a complete metallicity gap extending to zero frequency is still a challenge. We proposed a new method for the fabrication of layer-by-layer photonic crystals having metallic properties using silicon micromachining techniques. The touching layers form a

continuous network, where the long waves can not penetrate the conducting mesh, and the band gap extends to zero frequency. The method allows the fabrication of these structures at a frequency range extending from 100 GHz to 10 THz.

7.1 Fabrication Process

The new layer-by-layer photonic crystal was fabricated using highly doped silicon wafers. The resistivity of a silicon wafer decreases with the increasing doping concentration. We predicted that due to the low resistivity of Si wafers, this structure would show metallic photonic crystal properties. We have previously investigated the properties of a similar metallic photonic crystal with an upper band edge at 20 GHz. With the new scaled down dimensions, we expect this quasi-metallic photonic crystal to have a metallicity gap with an upper band edge around 100 GHz.

We used the anisotropic etching of silicon by aqueous potassium hydroxide (KOH) in forming the layers of the quasi-metallic photonic crystal. Using (100) silicon wafers, it is possible to etch arrays of parallel rods into wafers with rectangular cross-sections.⁷⁴ The (100) silicon wafers used in this work were each 75 mm in diameter and 400 μm thick. The resistivity of the wafers were in the range of 0.0015-0.004 $\Omega\text{-cm}$. In the first step of the process, one side of the wafers were coated with a silicon nitride film of thickness 1 μm , at 250°C using plasma enhanced chemical vapor deposition (PECVD) [Fig. 7.1(a)]. The nitride film serves as a mask during the anisotropic etching step, and we found out that this thickness was suitable for this purpose. Next, the nitride film was patterned by conventional photolithography and aqueous hydrofluoric acid (HF) etching. The pattern consists of 19 parallel stripes, each 950 μm wide and with center-to-center separation of 1600 μm . These stripe dimensions and the wafer thickness determine the upper band-edge, calculated to be around 100 GHz after the KOH etch.

The stripes are at an angle of 45° to the 110 plane of the silicon (as defined by the major flat of the wafer), which is simply the (010) direction of the wafer. This direction

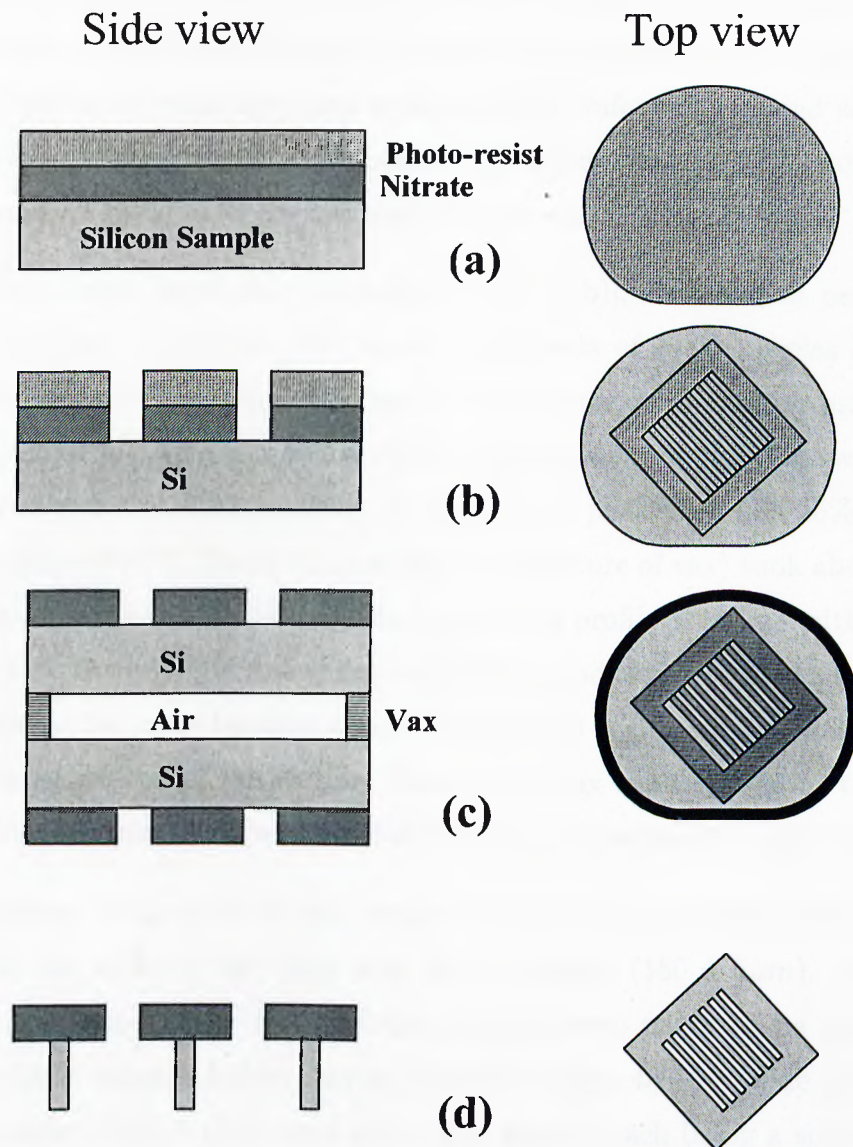


Figure 7.1: (a) In the first step, silicon nitride is deposited and photoresist is spun on the silicon wafer. (b) The nitride was patterned by conventional photolithography and aqueous hydrofluoric acid etching. (c) The resist is removed (by acetone), and two wafers are bonded together back-to-back by vax (d) Uncovered silicon surfaces are etched entirely through the wafer in KOH solution (left side). The photonic crystal layers are ready after the removal of nitride by HF solution (right side).

was chosen so that during the KOH etch, due to etching profile, the side walls of the rods (the $\{010\}$ planes) will always remain perpendicular to the etched surface (the $\{100\}$ planes). This way, the resulting rods of each layer will have rectangular cross-sections.⁷⁴ A 1.5 cm wide border around the stripe-array was protected by the photoresist to hold the rods of the layer, with the outer regions of the wafer left exposed so that a square will be left after etching. Within the border region were four small rectangular openings that will serve as guide holes for the stacking process.

After the nitride layer was patterned [Fig. 7.1(b)], in order to protect the back sides of the wafers, we covered the most outer parts of each samples back side with black wax (Apiezon-W). We than bonded it back-to-back with another patterned sample [Fig. 7.1(c)]. This way, the samples could then be etched in couples. The wafers were then dipped into an aqueous KOH solution. A typical etch performed in a 25% KOH solution at a temperature of 55°C (below the melting temperature of wax) took about 24 hours to etch entirely through the wafers. Due to the etching profile of silicon with KOH, during the 400 μm etch through the wafer, the width of the rods reduced the same amount from both side walls. So, rods became approximately $950 - (2 \times 400) = 150\mu\text{m}$ wide, and 400 μm thick at the end of the etching. Finally, the wax was removed by trichloroethane (TCA), and so the coupled layers bonded with wax are separated [Fig. 7.1(d), left side].

The thickness of the rods of each etched sample were measured with a microscope. We observed the width of the rods were fairly uniform ($150 \pm 5\mu\text{m}$). The remaining nitride film was removed by HF, and the samples were ready to be stacked to form photonic crystals using a holder having pins that align to the guide holes that were etched into wafers [Fig. 7.1(d), right side]. The wafers (each being a single layer of the quasi-metallic photonic crystal) may be stacked to form simple tetragonal (st) or face centered tetragonal (fct) type of crystals (see Fig. 6.1).

7.2 Characterization

Once the fabrication was completed, transmission properties of the crystal were measured with a W-band (75-120 GHz) measurement setup. A Ku-band frequency synthesizer was used to generate the signal that was first amplified and then multiplied in frequency by six times to reach the W band. The high frequency signal was radiated by a standard-gain horn antenna (aperture size of $1.17\text{cm} \times 1.45\text{cm}$), and the transmitted radiation was collected by a second horn antenna. The amplitude of the received signal was measured using a harmonic mixer and a network analyzer (Fig. 7.2).

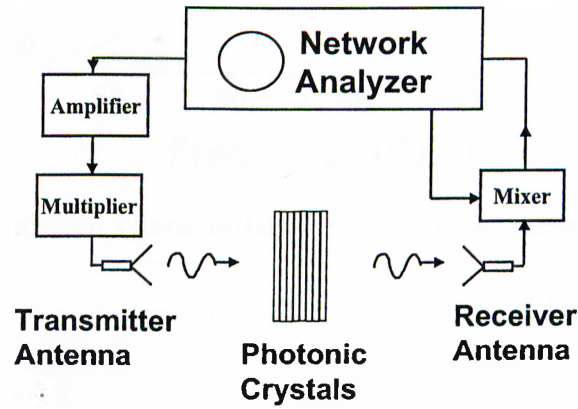


Figure 7.2: W-band experimental setup.

We measured the transmission spectra of st (Fig. 7.3) and fct (Fig. 7.4) structures as the number of layers are increased. The upper edge of the band gap for st crystal is located at 100 GHz, and for fct crystal at 115 GHz. No lower band edge is detected within the measurable frequency range, consistent with the theory that predicted a band gap extending down to zero frequencies. This metallicity gap verifies the prediction that our crystals are analogous to metallic photonic crystals and hence can be called quasi-metallic photonic crystals. At 80 GHz, the attenuation per layer is around 3.5 dB for st structure, 5.3 dB for fct structure. Within the metallicity gap of both of the crystals, we observe full reflection (100%) of the EM waves. The reflection spectra of the st type of

crystal is demonstrated in Fig. 7.5. We have simulated the transmission characteristics of these structures using TMM technique. Figure 7.6 shows the transmission from 4 layer st type of crystal (solid line), which agrees well with the TMM simulation results (dotted line).

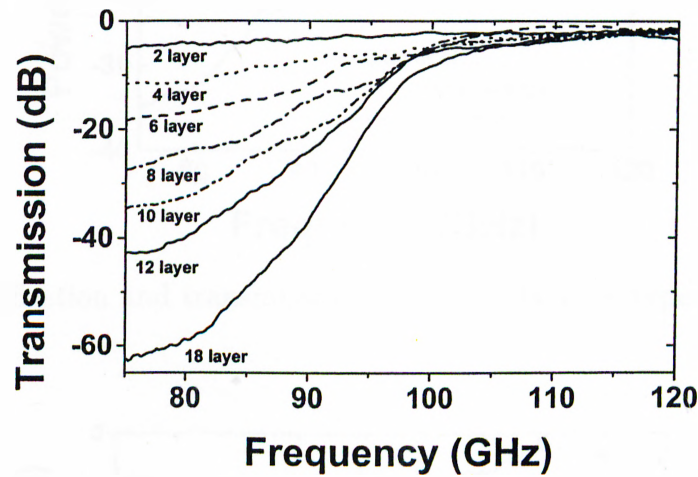


Figure 7.3: The transmission characteristics of st crystal structure as the number of layers are increased.

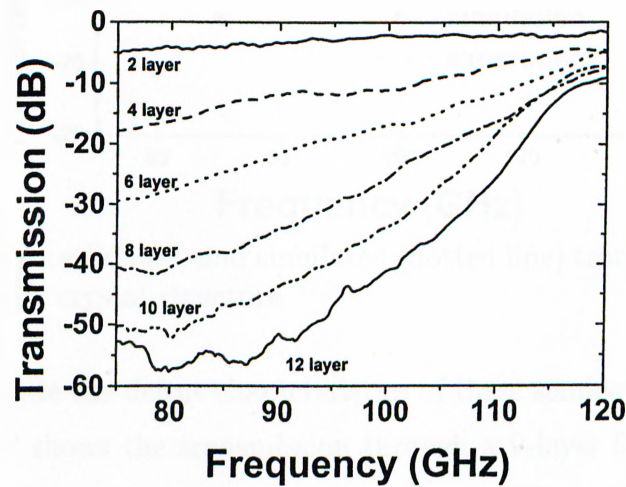


Figure 7.4: The transmission characteristics of fct crystal structure as the number of layers are increased.

We have previously shown that defect structures around this geometry can be built by means of adding or removing rods from an otherwise perfect crystal. The same idea

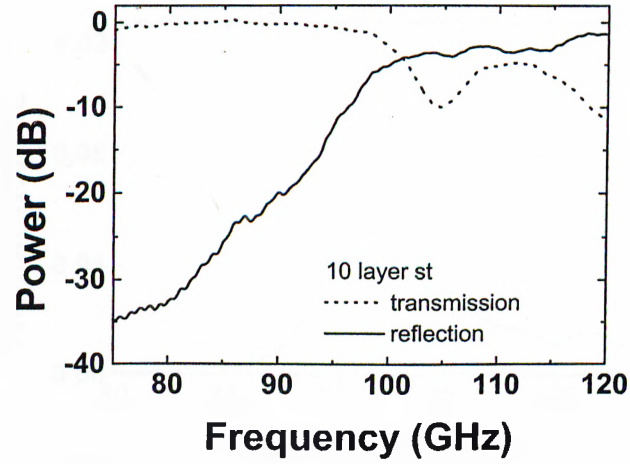


Figure 7.5: Reflection and transmission from a ten layer st type photonic crystal.

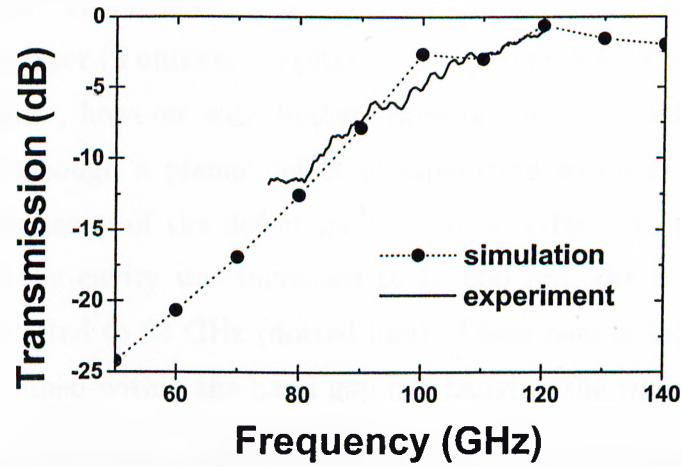


Figure 7.6: Measured (solid line) and simulated (dotted line) transmission characteristics of a four layer st type crystal structure

was used to investigate the defect characteristics of these semiconductor based photonic crystals. Figure 7.7 shows the transmission through a 9-layer fct type of crystal, with a single rod missing from the 5th layer of the crystal. The resonance frequency of the defect mode is at 91.8 GHz, with a Q-factor of 30.

We then investigated a planar type of defect structures, built around an 8-layer fct based photonic crystal. The planar defect was obtained by separating the 4th and 5th

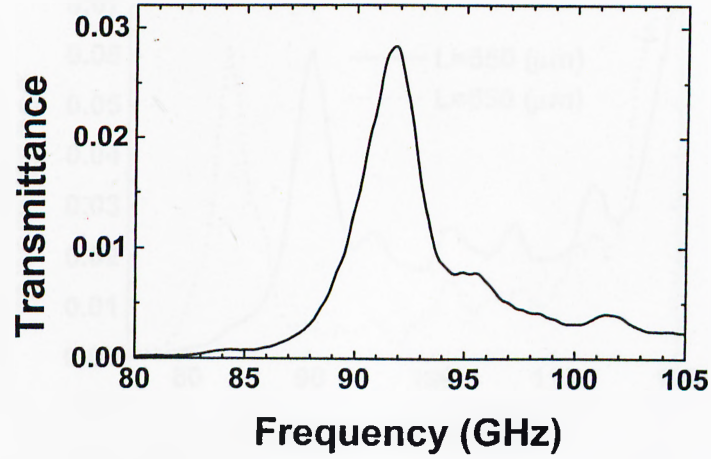


Figure 7.7: Transmission characteristics of 9 layer fct type of crystal with a single rod removed defect.

layers of the crystal. This resulted in a planar air gap between the two photonic mirrors, each formed of a 4 layer (2 unit cell) crystal. These planar defects also resulted in similar defect characteristics, however with higher transmission amplitudes. Figure 7.8 shows the transmission through a planar defect of separation width $L=550 \mu\text{m}$ (solid line). The resonance frequency of the defect mode is at 90 GHz with a Q-factor of 25. As the separation of the cavity was increased to $L=650 \mu\text{m}$, the resonance frequency of the defect mode shifted to 83 GHz (dotted line). These results indicate that the defect frequency can be tuned within the band gap by changing the width of the cavity.

In order to understand the effect of doping concentration to defect characteristics, we compared our experimental results with the TMM simulations performed by M. Sigalas of ISU (Fig. 7.9). We used the same planar defect structure described above, with a separation width of $800 \mu\text{m}$. The results of the simulations for a doping concentration of 10^{17} cm^{-3} , which corresponds to a resistivity of $0.09 \Omega\text{-cm}$, is shown as triangles in Fig. 7.9. As the doping concentration is increased to 10^{19} cm^{-3} (resistivity of $0.006 \Omega\text{-cm}$), the simulation results showed a significant increase in the Q-factor and the transmission amplitude of the defect mode (Fig. 7.9, circles). The resistivity of our wafers are still smaller (in the range of $0.0015\text{-}0.004 \Omega\text{-cm}$), and as shown in the Fig. 7.9,

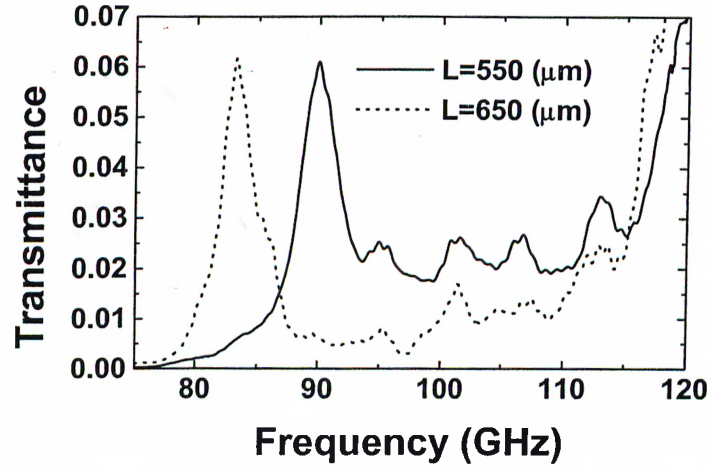


Figure 7.8: Transmission characteristics of 8 layer fct type of crystal with planar defect of separation $L = 550 \mu\text{m}$ (solid line) and $L = 650 \mu\text{m}$ (dotted line).

solid line, the measured transmission amplitude and the Q-factor is higher, as expected due to higher doping concentration (lower resistivity). The simulation results of a complete metallic structure, which is shown as squares, indicate that our results may still be improved to reach better defect characteristics using wafers with higher doping concentrations.

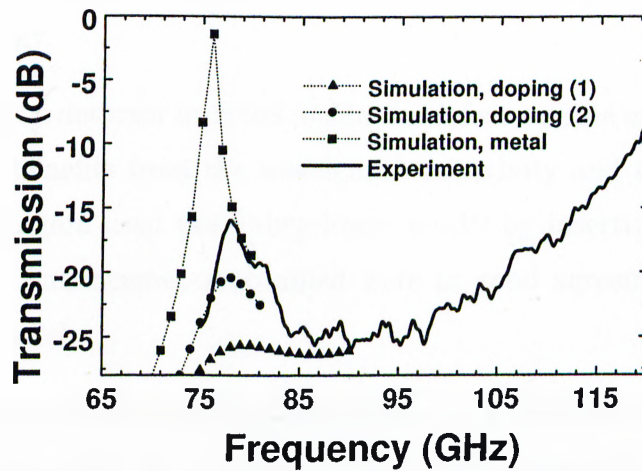


Figure 7.9: Calculated transmission spectra of a planar defect for two different doping concentrations (circles and triangles), for complete metallic structure (squares) and experimental result of the same defect structure (solid line).

Chapter 8

Conclusion

In this thesis work, we investigated the basic characteristics of dielectric and metallic photonic crystals. Using the transmission and reflection properties and the defect characteristics, we showed that photonic crystals are suitable for a number of applications, namely sensitive and frequency selective RCE detectors, highly directional resonance antennas, and waveguides.

We first investigated the reflection properties of the photonic crystals, and used this information to understand the defect formation for the planar defect structures with a Fabry-Perot analogy.

We showed that a detector inserted inside the defect volume of the cavity built around photonic crystals benefits from the wavelength selectivity and the large enhanced field of the cavity. We again used the Fabry-Perot model by inserting an absorption region inside the cavity. Enhancements obtained were in good agreement with the predicted values from the model.

We investigated the radiation characteristics of a photonic crystal-based antenna. The maximum directivity we measured, which was around 310, is very high when compared to the previously reported directivities of photonic crystal based antennas. There is an excellent agreement between the measurements and the FDTD calculations.

We have experimentally verified that EM wave can be guided with 100% transmission, using three dimensional photonic crystals. We have developed a parallel-plate waveguide model for our structures. The dispersion diagrams calculated using the transmitted phase measurements and by the waveguide model were in good agreement. We also observed 35% transmission for the EM waves travelling through a sharp bend in an L-shaped waveguide. We think that this value does not show the real transmission through the sharp bend. We believe that we can measure the exact percentage by either coupling the EM wave properly into the waveguide, or by measuring the magnitude of the guided EM wave within the waveguide before and after the sharp 90° bend. Another type of waveguide was also demonstrated, where the wave propagates through a missing rod within the crystal. We observed full transmission of the EM waves through this waveguide, and through an L-shaped waveguide constructed by crossing waveguides of the adjacent layers.

We showed that for certain requirements, metallic photonic crystals are more suitable when compared with dielectric-based photonic crystals. Their high rejection ratios and the wide metallicity gap with no lower frequency limit are suitable for many applications. We observed high Q factors and high transmission amplitudes from defect structures, and demonstrated two sample applications: RCE detectors and highly directional resonant antennas built around metallic photonic crystals.

We proposed and demonstrated a new method to fabricate quasi-metallic photonic crystals using silicon wafers. Measurements performed with the highly doped silicon micromachined layers exhibited metallicity gaps which agreed well with the TMM simulations. The defect transmission amplitudes and Q factors were lower when compared to previous metallic structures. The TMM simulation results show that, using wafers with higher doping concentrations, we can achieve better defect characteristics.

The search for new methods for fabrication of photonic crystals, and the characterization of them will certainly continue at all frequencies, since lots of undiscovered physics and an increasing number of applications are on the way.

Bibliography

- [1] These mirrors are exhibited in Anatolian Civilization Museum, Ankara, Turkey.
- [2] S. John, "Localization of Light," *Physics Today*, May 1991, p.32.
- [3] S. John, "The Localization of Light," NATO Advanced Science Institute on *Localization and Propagation of Classical Waves in Random and Periodic Structures*, held May 1992, Crete, GREECE, Plenum Publ. Corp. (1993).
- [4] S. John, "Strong Localization of Photons in Certain Disordered Dielectric Superlattices," *Phys. Rev. Lett.* **58**, 2486 (1987).
- [5] E. Yablonovitch, "Inhibited Spontaneous Emission in Solid-State Physics and Electronics," *Phys. Rev. Lett.* **58**, 2059 (1987).
- [6] P. R. Villeneuve, S. Fan, J. D. Joannopoulos, K. Y. Lim, G. S. Petrich, L. A. Kolodziejski, and R. Reif, "Air-Bridge Microcavities," *Appl. Phys. Lett.* **67**, 167 (1995).
- [7] P. L. Gourley, J. R. Wendt, G. A. Vawter, T. M. Brennan, and B. E. Hammons, "Optical Properties of Two Dimensional Photonic Lattices Fabricated as Honeycomb Nanostructures in Compound Semiconductors," *Appl. Phys. Lett.* **64**, 687 (1994).
- [8] J. P. Dowling, M. Scalora, M. J. Bloemer, and J. M. Bowden, "The Photonic Band Edge Laser: A New Approach to Gain Enhancement," *Appl. Phys. Lett.* **75**, 1896 (1994).

- [9] E. R. Brown, C. D. Parker, and E. Yablonovitch, "Radiation Properties of a Planar Antenna on a Photonic-Crystal Substrate," *J. Opt. Soc. Am. B* **10**, 404 (1993).
- [10] E. R. Brown, and O. B. McMahon, "High Zenithal Directivity from a Dipole Antenna on a Photonic Crystal," *Appl. Phys. Lett.* **68**, 1300 (1996).
- [11] C. J. Maggiore, A. M. Clogston, G. Spalek, W. C. Sailor, and F. M. Mueller, "Low-Loss Microwave Cavity Using Layered-Dielectric Materials," *Appl. Phys. Lett.* **64**, 1451 (1994).
- [12] D. R. Smith, S. Shultz, N. Kroll, M. Sigalas, K. M. Ho, and C. M. Soukoulis, "Experimental and Theoretical Results for a Two-Dimensional Metal Photonic Band-Gap Cavity," *Appl. Phys. Lett.* **65**, 645 (1994).
- [13] B. Temelkuran, E. Ozbay, J. P. Kavanaugh, G. Tuttle, and K. M. Ho, "Resonant Cavity Enhanced Detectors Embedded in Photonic Crystals," *Appl. Phys. Lett.* **72**, 2376 (1998).
- [14] M. Thevenot, C. Cheype, A. Reineix, and B. Jecko, "Directive Photonic-Bandgap Antennas," *IEEE Trans. Microwave theory Tech.* **47**, 2115 (1999).
- [15] B. Temelkuran and E. Ozbay, "Experimental Demonstration of Photonic Crystal Based Waveguides," *Appl. Phys. Lett.* **74**, 486 (1999).
- [16] S. H. Fan, P. R. Villeneuve, J. D. Joannopoulos, H. A. Haus, "Channel Drop Filters in Photonic Crystals," *Opt. Express* **3**, 4 (1998).
- [17] E. Yablonovitch, "Photonic Band-Gap Structures," *J. Opt. Soc. Am. B* **10**, 283 (1993).
- [18] E. Yablonovitch, T. J. Gmitter, R. D. Meade, A. M. Rappe, K. D. Brommer, and J. D. Joannopoulos, "Donor and Acceptor Modes in Photonic Band Structure," *Phys. Rev. Lett.* **67**, 3380 (1991).
- [19] J. D. Joannopoulos, R. D. Meade, and J. N. Winn, *Photonic Crystals: Molding the Flow of Light*, (Princeton University Press, Princeton, NJ, 1995).

- [20] "Lasing Demonstrated in Tiny Cavities Made with Photonic Crystals," *Physics Today*, September 1999, p. 20.
- [21] O. Painter, R. K. Lee, A. Scherer, A. Yariv, J. D. O'Brien, P. D. Dapkus, and I. Kim, "Two-Dimensional Photonic Band-Gap Defect Mode Laser," *Science* **284**, 1819 (1999).
- [22] K. M. Ho, C. T. Chan, and C. M. Soukoulis, "Existence of a Photonic Band Gap in Periodic Structures," *Phys. Rev. Lett.* **65**, 3152 (1990).
- [23] E. Yablonovitch, and K. M. Leung, "Photonic Band Structure: Non-Spherical Atoms in the Face-Centered Case," *Physica B* **175**, 81 (1991).
- [24] K. M. Leung, and Y. F. Liu, "Full Vector Wave Calculation of Photonic Band Structures in Face-Cubic-Centered Dielectric Media," *Phys. Rev. Lett.* **65**, 2646 (1990).
- [25] Z. Zhang, and S. Satpathy, "Electro-Magnetic wave Propagation in Periodic Structures: Bloch Wave Solutions of Maxwell's Equations," *Phys. Rev. Lett.* **65**, 2650 (1990).
- [26] K. M. Ho, C. T. Chan, C. M. Soukoulis, R. Biswas, and M. M. Sigalas, "Photonic Band Gaps in Three Dimensions: New Layer-by-Layer Periodic Structures," *Solid State Commun.* **89**, 413 (1994).
- [27] E. Ozbay, A. Abeyta, G. Tuttle, M. Tingides, R. Biswas, C. T. Chan, C. M. Soukoulis, and K. M. Ho, "Measurement of a Three-Dimensional Photonic Band Gap in a Crystal Structure Made of Dielectric Rods," *Phys. Rev. B* **50**, 1945 (1994).
- [28] E. Ozbay, E. Michel, G. Tuttle, R. Biswas, M. M. Sigalas, and K. M. Ho, "Micromachined Millimeter-Wave Photonic Band-Gap Crystals," *Appl. Phys. Lett.* **64**, 2059 (1994).

- [29] E. Ozbay, E. Michel, G. Tuttle, R. Biswas, M. M. Sigalas, K. M. Ho, J. Bostak and D. M. Bloom, "Terahertz Spectroscopy of Three-dimensional Photonic Band-Gap Crystals," *Opt. Lett.* **19**, 951 (1994).
- [30] E. Ozbay, G. Tuttle, R. Biswas, K. M. Ho, J. Bostak and D. M. Bloom, "Double-etch Geometry for Millimeter-Wave Photonic Band-Gap Crystals," *Appl. Phys. Lett.* **65**, 1617 (1994).
- [31] S. Y. Lin, J. G. Fleming, M. M. Sigalas, R. Biswas, and K. M. Ho, "A three-dimensional photonic crystal operating at infrared wavelength," *Nature (London)* **394**, 251 (1998).
- [32] S. Y. Lin and J. G. Fleming, "A Three-Dimensional Optical Photonic Crystal," *J. Lightwave Technol.* **17**, 1944 (1999).
- [33] J. G. Fleming and S. Y. Lin, "Three-dimensional photonic crystal with a stop band from 1.35 to 1.95 μm ," *Opt. Lett.* **24**, 49 (1999).
- [34] S. Noda, N. Yamamoto, H. Kobayashi, M. Okano, and K. Tomoda, "Optical properties of Three-Dimensional Photonic Crystals Based on III-V Semiconductors at Infrared to Near-Infrared Wavelengths," *Appl. Phys. Lett.* **75**, 905 (1999).
- [35] S. Noda, "Three-Dimensional Photonic Crystals Operating at Optical Wavelength Region," *Physica B* **279** 142 (2000).
- [36] E. Ozbay, and B. Temelkuran, "Reflection Properties and Defect Formation in Photonic Crystals," *Appl. Phys. Lett.* **69**, 743 (1996).
- [37] A. E. Siegman, *Lasers*, (University Science Books, 1986).
- [38] M.S. Ünlü, "Resonant Cavity Enhanced Photonic Devices," *J. Appl. Phys.* **78**, 1 (1995).
- [39] M. M. Sigalas, R. Biswas, Q. Li, D. Crouch, W. Leung, R. Jacobs-Woodbury, B. Lough, S. Nielsen, S. McCalmont, G. Tuttle, and K. M. Ho, "Dipole Antennas on

- Photonic Band-Gap Crystals: Experiment and Simulation,” *Micro. Opt. Tech. Lett.* **15**, 153 (1997).
- [40] R. Gonzalo, Peter de Maagt, and M. Sorolla, “Enhanced Patch-Antenna Performance by Suppressing Surface Waves Using Photonic-Bandgap Substrates,” *IEEE Trans. Microwave theory Tech.* **47**, 2131 (1999).
- [41] G. Poilasne, P. Pouliguen, K. Mahdjoubi, J. Lenormand, C. Terret, and Ph. Gelin, “Theoretical Study of Grating Lobes Reduction Using Metallic Photonic Bandgap Materials (MPBG),” *Micro. Opt. Tech. Lett.* **18**, 32 (1998).
- [42] B. Temelkuran, Mehmet Bayindir, E. Ozbay, R. Biswas, M. M. Sigalas, G. Tuttle, and K. M. Ho, “Photonic Crystal Based Resonant Antenna with a very High Directivity,” *J. Appl. Phys.* **87**, 603 (2000).
- [43] A. Yariv and P. Yeh, *Optical Waves in Crystals*, (Wiley, New York, 1984).
- [44] E. F. Schubert, N. E. J. Hunt, A. M. Vredenberg, T. D. Harris, J. M. Poate, D. C. Jacobson, Y. H. Wong, and G. J. Zyzdik, “Increased Fiber Communications Bandwidth from a Resonant Cavity Light Emitting Diode Emitting at $\lambda = 940$ nm,” *Appl. Phys. Lett.* **63**, 2603 (1993).
- [45] M. M. Sigalas, R. Biswas, K. M. Ho, C. M. Soukoulis, and D. D. Crouch, “Waveguides in Three-Dimensional Metallic Photonic Band-Gap Materials,” *Phys. Rev. B* **60**, 4426 (1999).
- [46] Shawn-Yu Lin, E. Chow, V. Hietala, P. R. Villeneuve, and J. D. Joannopoulos, “Experimental Demonstration of Guiding and Bending of Electromagnetic Waves in a Photonic Crystal,” *Science* **282**, 274 (1998).
- [47] I. El-kady, M. M. Sigalas, R. Biswas, and K. M. Ho, “Dielectric Waveguides in Two-Dimensional Photonic Bandgap Materials,” *J. Lightwave Technol.* **17**, 2042 (1999).

- [48] B. Temelkuran, E. Ozbay, M. Sigalas, G. Tuttle, C. M. Soukoulis, and K. M. Ho, "Reflection Properties of Metallic Photonic Crystals," *Appl. Phys. A* **66**, 363 (1998).
- [49] J. D. Jackson, *Classical Electrodynamics*, 2nd ed., (Wiley, New York, 1975).
- [50] A. Chutinan and S. Noda, "Highly Confined Waveguides and Waveguide Bends in Three-Dimensional Photonic Crystal," *Appl. Phys. Lett.* **75**, 3739 (1999).
- [51] M. M. Sigalas, R. Biswas, K. M. Ho, C. M. Soukoulis, D. Turner, B. Vasiliu, S. C. Kothari, and S. Lin, "Waveguide Bends In Three-Dimensional Layer-by-Layer Photonic Bandgap Materials," *Microw. Opt. Techn. Lett.* **23**, 56 (1999).
- [52] N. Stefanou and A. Modinos, "Impurity Bands in Photonic Insulators," *Phys. Rev. B* **57**, 12127 (1998).
- [53] A. Yariv, Y. Xu, R. K. Lee, and A. Scherer, "Coupled-Resonator Optical Waveguide: A Proposal and Analysis," *Opt. Lett.* **24**, 711 (1999).
- [54] Mehmet Bayindir, B. Temelkuran, and E. Ozbay, "Tight-Binding Description of the Coupled Defect Modes in Three-Dimensional Photonic Crystals," *Phys. Rev. Lett.* **84**, 2140 (2000).
- [55] Mehmet Bayindir, B. Temelkuran, and E. Ozbay, "Propagation of Photons via Hopping: A Novel Waveguiding Mechanism Through Localized Coupled-Cavities in Three-Dimensional Photonic Crystals," *Phys. Rev. B* **61**, p.**** (May 2000).
- [56] M. M. Sigalas, C. T. Chan, K. M. Ho, and C. M. Soukoulis, "Metallic Photonic Band-Gap Materials," *Phys. Rev. B* **52**, 11744 (1995).
- [57] S. McCalmont, M. Sigalas, G. Tuttle, and K. M. Ho, "A Layer-by-Layer Metallic Photonic Band Gap Structure," *Appl. Phys. Lett.* **68**, 2759 (1996).
- [58] D. F. Sievenpiper, M. E. Sickmiller, and E. Yablonovitch, "3-D Wire Mesh Photonic Crystals," *Phys. Rev. Lett.* **76**, 2480 (1996).

- [59] E. Ozbay, B. Temelkuran, M. M. Sigalas, G. Tuttle, C. M. Soukoulis, and K. M. Ho, "Defect Structures in Metallic Photonic Crystals," *Appl. Phys. Lett.* **69**, 3797 (1996).
- [60] B. Temelkuran, H. Altug, E. Ozbay, "Experimental Investigation of Layer-By-Layer Metallic Photonic Crystals," *IEE Proc.-Optoelectron.* **145**, 149 (1998).
- [61] J.B. Pendry and A. MacKinnon, "Calculation of Photon Dispersion Relation," *Phys. Rev. Lett.* **69**, 2772 (1992); J.B. Pendry, "Photonic Band Structures," *J. Mod. Opt.* **41**, 209 (1994).
- [62] E. Ozbay, G. Tuttle, M. M. Sigalas, C. M. Soukoulis, and K. M. Ho, "Defect Structures in a Layer-by-Layer Photonic Band-Gap Crystal," *Phys. Rev. B* **51**, 13961 (1995).
- [63] M. M. Sigalas, C. M. Soukoulis, C. T. Chan, and K. M. Ho, "Electromagnetic-Wave Propagation Through Dispersive and Absorptive Photonic-Band-Gap Materials," *Phys. Rev. B* **49**, 11080 (1994).
- [64] M. C. Wanke, O. Lehmann, K. Muller, Q. Wen, and M. Stuke, "Laser Rapid Prototyping of Photonic Band-Gap Microstructures," *Science* **275**, 1284 (1997).
- [65] E. Ozbay, "Layer-by-Layer Photonic Crystals from Microwave to Far-Infrared Frequencies," *J. Opt. Soc. Am. B* **13**, 1945 (1996).
- [66] A. Kao, K. A. McIntosh, O. B. McMahon, R. Atkins, and S. Verghese, "Calculated and Measured Transmittance of Metallodielectric Photonic Crystals Incorporating Flat Metal Elements," *Appl. Phys. Lett.* **72**, 145 (1998).
- [67] W. Y. Leung, G. Tuttle, M. M. Sigalas, R. Biswas, K. M. Ho, and C. M. Soukoulis, "Optimizing the Q Value in Three-Dimensional Metallic Photonic Band Gap Crystals," *J. Appl. Phys.* **84**, 4091 (1998).

- [68] N. Katsarakis, E. Chatzitheodoridis, G. Kiriakidis, M. M. Sigalas, C. M. Soukoulis, W. Y. Leung, and G. Tuttle, "Laser-Machined Layer-by-Layer Metallic Photonic Band-Gap Structures", *Appl. Phys. Lett.* **74**, 3263 (1999).
- [69] G. Poilasne, P. Pouliguen, K. Mahdjoubi, C. Terret, P. Gelin, and L. Desclos, "Experimental Radiation Pattern of Dipole Inside Metallic Photonic Bandgap Material," *Microwave Opt. Technol. Lett.* **22**, 10 (1999).
- [70] M. J. Bloemer and M. Scalora, "Transmissive Properties of Ag/MgF₂ Photonic Band Gaps," *Appl. Phys. Lett.* **72**, 1676 (1998).
- [71] C. Jin, B. Cheng, Z. Li, D. Zhang, L. M. Li, and Z. Q. Zhang, "Two Dimensional Metallic Photonic Crystal in THz Range," *Opt. Commun.* **166**, 9 (1999).
- [72] S. Gupta, G. Tuttle, M. Sigalas, and K. M. Ho, "Infrared Filters Using Metallic Photonic Band Gap Structures on Flexible Substrates," *Appl. Phys. Lett.* **71**, 2412 (1997).
- [73] K. A. McIntosh, L. J. Mahoney, K. M. Molvar, O. B. McMahon, S. Verghese, M. Rothschild, and E. R. Brown, "Three-Dimensional Metallodielectric Photonic Crystals Exhibiting Resonant Infrared Stop Bands," *Appl. Phys. Lett.* **70**, 2937 (1997).
- [74] E. Bassous, "Anisotropic Etching of Silicon For 3-D Microstructure Fabrication," in *Symposium on Electrochemical Thecnology in electronics*, ed. by L. T. Romankiw and T. Osaka, (Electrochemical Society, Pennington, NJ, 1987), p.616.